buildings

MDPI

Article

Wear-Resistant Skid Resistance and Raveling Resistance of Ceramic Aggregate High-Viscosity Asphalt Mixtures

Bo Tan [1,2], Qi Zhen [1,2,*], Tianci Zhao [1,2], Wanzhen Zhang [1,2] and Lihao Zhu [1,2]

[1] Guangxi Key Laboratory of Green Building Materials and Construction Industrialization, Guilin University of Technology, Guilin 541004, China; 2000015@glut.edu.cn (B.T.); 1020220653@glut.edu.cn (T.Z.); 1020220687@glut.edu.cn (W.Z.); 2120251072@glut.edu.cn (L.Z.)
[2] School of Civil Engineering, Guilin University of Technology, Guilin 541004, China
* Correspondence: zhenqi@glut.edu.cn

Abstract

To address the rapid polishing and premature loss of skid resistance in conventional asphalt friction courses, as well as the weak bonding between waste ceramic aggregates and asphalt that compromises raveling resistance, this study developed a ceramic aggregate asphalt mixture incorporating TPS–SBS composite high-viscosity modified asphalt, denoted as T&S. The wear-retained skid resistance and raveling resistance of the mixture were systematically evaluated. Interfacial adhesion between the modified asphalt and ceramic aggregates was characterized using water-immersion adhesion and contact-angle tests. Mixtures with different ceramic aggregate contents were further investigated through laboratory-accelerated abrasion, immersion Cantabro particle loss, and torsional raveling tests. In addition, an empirical skid-resistance degradation model and a frictional impulse-based characterization model were established. The results showed that TPS increased the asphalt–ceramic aggregate adhesion grade from Grade 3 to Grade 5, indicating a marked improvement in interfacial adhesion. Mixture skid resistance increased with ceramic aggregate content. After 16 h of abrasion, the residual British pendulum number of the mixture containing 80% ceramic aggregates was 38.7% higher than that of the control mixture. However, a ceramic aggregate content of 40% was identified as a practical balance point between skid-resistance improvement and overall mixture performance under the present laboratory conditions. T&S-modified asphalt reduced both Cantabro particle loss and torsional mass loss by more than 40%, partly compensating for the interfacial and skeleton-interlocking limitations of ceramic aggregates. The proposed models achieved coefficients of determination (R^2) greater than 0.997, indicating high fitting accuracy for the present laboratory data. The preferred mixture design was determined as 8% TPS and 40% ceramic aggregate, providing a promising technical pathway for the resource utilization of construction-derived waste ceramics in asphalt pavements.

Keywords: high-viscosity asphalt; waste ceramic aggregate; asphalt mixture; wear-resistant skid performance; raveling resistance; accelerated abrasion test

Check for updates

Academic Editor: Antonio Caggiano

Received: 13 May 2026
Revised: 25 June 2026
Accepted: 27 June 2026
Published: 29 June 2026

Copyright: © 2026 by the authors. Licensee MDPI, Basel, Switzerland. This article is an open access article distributed under the terms and conditions of the Creative Commons Attribution (CC BY) license.

1. Introduction

Pavement skid resistance is closely related to vehicle braking efficiency and traffic safety and is particularly critical under wet weather conditions. According to statistics reported by the Ministry of Transport, more than 30% of traffic accidents on expressways in China are directly associated with insufficient pavement skid resistance [1]. Asphalt friction

courses have traditionally relied primarily on natural hard aggregates such as basalt [2]; however, under the combined effects of heavy traffic loading, repeated tire abrasion, and moisture intrusion, aggregate polishing [3], asphalt film stripping [4], surface raveling, and particle loss [5] are almost unavoidable, resulting in persistent safety risks. Therefore, the development of new pavement materials that combine excellent initial skid-resistant texture, long-term wear-retention performance, and strong raveling resistance has become a key challenge in road engineering [6–8].

Aggregates produced by crushing and processing waste ceramics are regarded as promising high-quality alternatives to natural skid-resistant aggregates because of their high hardness, with a Mohs hardness of 6–7, excellent abrasion resistance, and favorable physicochemical stability [9]. Previous studies have shown that, compared with basalt aggregates, incorporating ceramic aggregates into pavement surface layers can improve initial skid resistance, delay polishing, and provide a feasible pathway for the resource utilization of solid waste [10]. However, ceramic aggregates possess dense surfaces and relatively few polar functional groups. These intrinsic characteristics result in weak interfacial adhesion with conventional SBS-modified asphalt [11], making asphalt film stripping and aggregate detachment more likely during service and thereby limiting the broader technical application of ceramic aggregates in road engineering [12].

The TPS thermoplastic elastomer modifier can act synergistically with SBS polymers to form a stable interpenetrating network, thereby substantially improving the dynamic viscosity and cohesion of asphalt, as well as its wetting and spreading ability on aggregate surfaces [13,14]. In addition, polar active groups on TPS molecular chains may develop strong interfacial interactions, such as hydrogen bonding, polar adsorption, or chemical bonding, with inorganic aggregate surfaces, depending on the mineral composition and surface chemistry of the aggregate [15,16]. This provides a plausible pathway for improving ceramic–asphalt interfacial adhesion. Nevertheless, systematic studies integrating TPS–SBS composite high-viscosity asphalt with ceramic aggregates remain limited, and the synergistic enhancement mechanism, skid-resistance degradation behavior, and raveling resistance of this material system remain insufficiently understood.

From the perspective of sustainability, the value of ceramic waste as an asphalt-pavement aggregate lies not only in solid-waste consumption and substitution of natural resources, but also in the potential contribution of its high wear resistance to extending pavement service life [17]. Nevertheless, the use of recycled construction materials requires careful consideration of performance trade-offs, material variability, and durability limits [18]. Previous studies have shown that recycled aggregates exhibit substantially greater variability than natural aggregates in apparent density, water absorption, pore structure, and surface chemistry; such variability should therefore be fully considered during mixture design [19,20]. On the basis of material characterization, systematic pavement performance evaluation, and optimum dosage determination, this study preliminarily defines the performance boundary of the proposed material system. A quantitative comparison of life-cycle environmental benefits and costs should be further conducted in future work.

To address these research gaps, this study focuses on ceramic aggregate high-viscosity asphalt mixtures and systematically investigates their wear-resistant skid performance and raveling resistance. First, the key differences in interfacial adhesion between T&S composite high-viscosity modified asphalt and conventional SBS-modified asphalt on ceramic aggregate surfaces are compared using water-immersion adhesion tests [21]. Subsequently, a series of high-viscosity asphalts with different TPS dosages are prepared, and the optimum dosage is determined through systematic evaluation of conventional pavement-related properties, aging characteristics, and high-viscosity rheological indices. On this basis,

mixtures with different ceramic aggregate replacement ratios are prepared. After their conventional properties, including high-temperature stability, moisture stability, and indirect tensile strength, are evaluated, laboratory-accelerated abrasion [22], immersion Cantabro particle loss [23], and torsional raveling tests are conducted to further elucidate the wear-induced skid-resistance degradation mechanism and raveling resistance under multiple service conditions. In addition, an empirical skid-resistance degradation model and a frictional impulse-based characterization model are established. This study aims to provide systematic theoretical evidence and experimental support for the technical application of ceramic aggregate high-viscosity asphalt mixtures in long-life skid-resistant pavements, while also providing laboratory evidence for the technical application of construction-derived waste ceramics in asphalt pavements.

2. Materials and Test Methods

2.1. Materials

SBS-modified asphalt, Type I-D, was supplied by Maoming Lusheng Asphalt Co., Ltd., Maoming, China, and its main technical properties are listed in Table 1.

Table 1. Technical properties of SBS-modified asphalt, Type I-D.

Property		Unit	Measured Value	Specification Requirement
Penetration, 25 °C		0.1 mm	54	40–60
Softening point, TR&B		°C	72	≥60
Ductility, 5 °C		cm	28	≥20
Relative density of asphalt		g·cm^{-3}	1.033	Measured
Dynamic viscosity, 60 °C		Pa·s	2343	Measured
Elastic recovery, 25 °C		%	80	≥75
Flash point		°C	275	≥230
RTFOT, 163 °C	Mass loss	%	−0.5	≤±0.1
	Retained penetration ratio	%	72	≥65
	Ductility, 5 °C	cm	16	≥15

The TPS thermoplastic elastomer modifier was primarily composed of thermoplastic rubber, tackifying resin, plasticizer, and other blended components [24], as shown in Figure 1a. Among these components, thermoplastic rubber provides excellent elastic recovery, tackifying resin enhances the interfacial bonding between asphalt and aggregates, and the plasticizer improves processing fluidity. Through the synergistic action of these components, conventional asphalt can be converted into a high-viscosity binder during mechanical mixing.



(**a**) (**b**)

Figure 1. (**a**) TPS modifier and (**b**) ceramic aggregate.

The ceramic aggregates were derived from waste generated during the production of daily-use ceramic products by Wuzhou Tengxian Xinzhongtao Co., Ltd., Wuzhou, China and their major chemical composition is listed in Table 2. After primary crushing using a jaw crusher and secondary crushing using an impact crusher, ceramic particles with a size range of 4.75–9.5 mm were screened and used as recycled aggregates, as shown in Figure 1b. The average surface roughness Ra of the ceramic aggregates, measured using laser confocal microscopy, was approximately 5.2 ± 0.8 μm, compared with 8.7 ± 1.3 μm for the limestone aggregates. Their main technical properties are listed in Table 3.

Table 2. Chemical composition of ceramic aggregates (XRF analysis).

Oxide	SiO_2	Al_2O_3	K_2O	Na_2O	CaO	MgO	Fe_2O_3	TiO_2	LOI	Total
Content (wt%)	68.5	19.2	3.8	2.1	1.5	0.8	1.2	0.4	1.8	99.3
Variation range (wt%)	64–73	16–22	2.5–5.0	1.0–3.5	0.5–3.0	0.3–1.5	0.5–2.0	0.2–0.8	0.5–3.0	-

Table 3. Technical properties of ceramic aggregates.

Test Item		Test Result	Specification Requirement	Test Method
Apparent relative Density/g·cm^{-3}	4.75–9.5 mm	2.443	≥2.6	T0304
Water absorption/%	4.75–9.5 mm	0.86	≤2	
Crushing value/%		19.50	≤28	T0316
Los Angeles abrasion value/%		18.80	≤30	T0317
Flat and elongated particle content/%		13.70	≤15	T0312

Limestone aggregates were obtained from the Lingui Mixing Plant in Guilin and were divided into four size fractions: 0–2.36 mm, 2.36–4.75 mm, 4.75–9.5 mm, and 9.5–13.2 mm. Their main technical properties are presented in Table 4.

Table 4. Technical properties of limestone aggregates.

Test Item	Particle Size	Test Result	Specification Requirement	Test Method
Apparent relative density/g·cm^{-3}	13.2–9.5 mm	2.72	≥2.6	T0304
	9.5–4.75 mm	2.718		
	4.75–2.36 mm	2.716		
	0–2.36 mm	2.695	≥2.5	T0328
Water absorption/%	13.2–9.5 mm	0.33	≤2	T0308
	9.5–4.75 mm	0.44		
	4.75–2.36 mm	0.79		
Crushing value/%	9.5–4.75 mm	24.10	≤26	T0316
Los Angeles abrasion value/%	9.5–4.75 mm	24.40	≤28	T0317
Flat and elongated particle content/%	9.5–4.75 mm	6.60	≤15	T0312

The mineral filler was prepared from limestone fine aggregates through screening and processing, and its main technical properties are shown in Table 5.

Table 5. Technical properties of mineral filler.

Test Item	Test Result	Specification Requirement	Test Method
Apparent density/g·cm^{-3}	2.694	≥2.45	T0352
Water content/%	0.60	≤1	T0103

Table 5. *Cont.*

Test Item	Test Result	Specification Requirement	Test Method
Particle size < 0.6 mm	100%	100%	T0351
Particle size < 0.15 mm	98.68%	90–100%	
Particle size < 0.075 mm	80.60%	70–100%	

2.2. Preparation of Composite High-Viscosity Modified Asphalt

The compounding of the TPS modifier and SBS-modified asphalt was mainly achieved through physical blending. Under high-temperature shearing, TPS is adsorbed onto the SBS molecular chains, and the two components form an obliquely interlaced linear fibrous network structure, which provides the structural basis for the marked increase in the viscosity of the composite modified asphalt. In this study, the TPS dosages were set at 5%, 8%, and 11%, which were denoted as T&S-5, T&S-8, and T&S-11, respectively. The preparation procedure for the T&S modified asphalt is illustrated in Figure 2.



Figure 2. Preparation procedure for T&S modified asphalt.

2.3. Mixture Design and Optimum Asphalt–Aggregate Ratio

In this study, a stone asphalt concrete, SAC, gradation was adopted. This gradation forms a coarse aggregate interlocking skeleton and provides a relatively large surface texture depth, thereby offering both favorable skid resistance and deformation resistance. The combined gradation curve of the SAC-10 ultra-thin wearing course and the corresponding specification limits are shown in Figure 3.

Ceramic aggregates were used to replace limestone coarse aggregates at equal-volume replacement ratios of 0%, 20%, 40%, 60%, and 80%, which effectively eliminated the interference of density differences with the gradation skeleton structure. Meanwhile, the crushing value and Los Angeles abrasion value of the ceramic aggregates both satisfied the specification requirements, providing a basic guarantee for the mechanical stability of the aggregate skeleton. The optimum asphalt–aggregate ratio was determined using the Marshall method. Based on practical experience, the asphalt–aggregate ratio of SAC-10 generally falls within the range of 4.5–6.0%. Five asphalt–aggregate ratio levels, ranging from 4.0% to 6.0% at intervals of 0.5%, were selected. Four standard Marshall specimens were prepared for each group, with a target air-void content of 4%. Bulk specific gravity and Marshall stability tests

were then conducted on the compacted specimens, and the optimum asphalt–aggregate ratio for each ceramic aggregate content was determined comprehensively. The main test results are summarized in Tables 6 and 7.

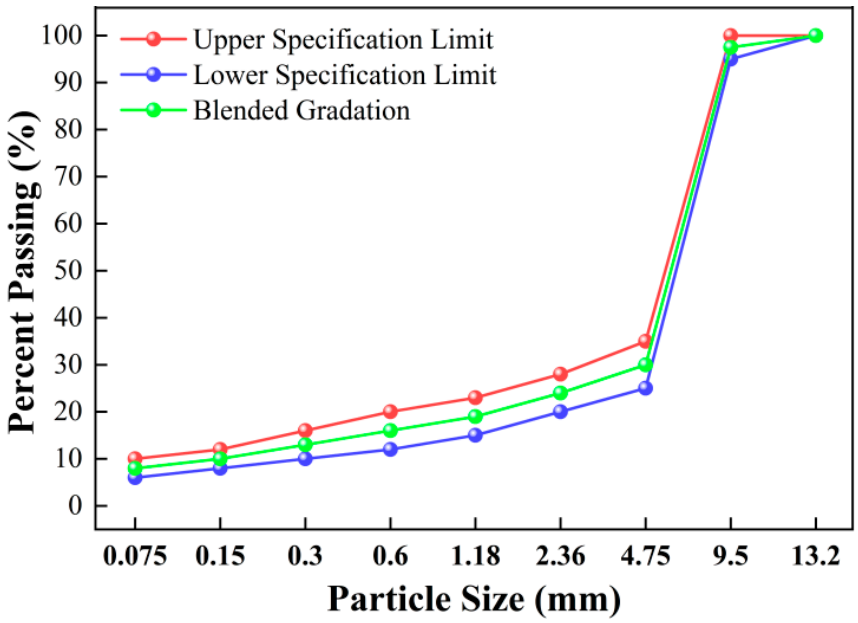


Figure 3. Gradation range of the SAC-10 ultra-thin wearing course.

Table 6. Marshall test results of ceramic aggregate T&S asphalt mixtures.

Ceramic Aggregate Content/%	0%	20%	40%	60%	80%
Optimum asphalt–aggregate ratio/%	4.3	4.5	4.8	5.4	6.1
Bulk specific gravity/g·cm^{-3}	2.436	2.379	2.325	2.268	2.201
Theoretical maximum specific gravity/g·cm^{-3}	2.527	2.477	2.420	2.364	2.295
Air voids/%	3.6	4.0	3.9	4.1	4.3
Voids filled with asphalt/%	73.9	72.9	72.1	72.8	74.2
Marshall stability/kN	19.63	19.96	17.49	14.81	10.85
Flow value/mm	24.2	26.5	28.1	31.7	34.5

Table 7. Marshall test results of ceramic aggregate SBS asphalt mixtures.

Ceramic Aggregate Content/%	0%	20%	40%	60%	80%
Optimum asphalt–aggregate ratio/%	4.7	4.9	5.2	5.6	6.3
Bulk specific gravity/g·cm^{-3}	2.412	2.353	2.311	2.258	2.195
Theoretical maximum specific gravity/g·cm^{-3}	2.513	2.461	2.415	2.370	2.302
Air voids/%	4.0	4.4	4.3	4.7	4.5
Voids filled with asphalt/%	73.3	71.4	71.0	70.6	69.8
Marshall stability/kN	11.75	10.11	8.36	7.45	5.62
Flow value/mm	31.4	33.0	35.2	38.5	42.0

2.4. Test Methods

The conventional properties of the asphalt binder were tested in accordance with the Standard Test Methods of Bitumen and Bituminous Mixtures for Highway Engineering (JTG E20-2011) [25]. Contact angles were measured using a CA500S contact-angle meter by the sessile-drop method, as shown in Figure 4a, and were calculated by fitting the droplet profile with the Young–Laplace equation. The dynamic viscosity at 60 °C was measured using a Shanghai Changji SYD-0620 asphalt dynamic viscosity tester, Shanghai, China,

as shown in Figure 4e. Aging resistance was evaluated using the rolling thin-film oven test (RTFOT), as shown in Figure 4d. High-temperature rutting resistance was tested using a Shanghai Changji SYD-0719A automatic rutting tester, as shown in Figure 4f. Moisture stability was evaluated using the immersion Marshall test, performed with a Shanghai Changji SYD-0709A Marshall stability tester, as shown in Figure 4b. Freeze–thaw splitting strength and indirect tensile strength were measured using an electronic universal testing machine manufactured by Shenzhen Sansi Zongheng Technology Co., Ltd., Shenzhen China, as shown in Figure 4c.

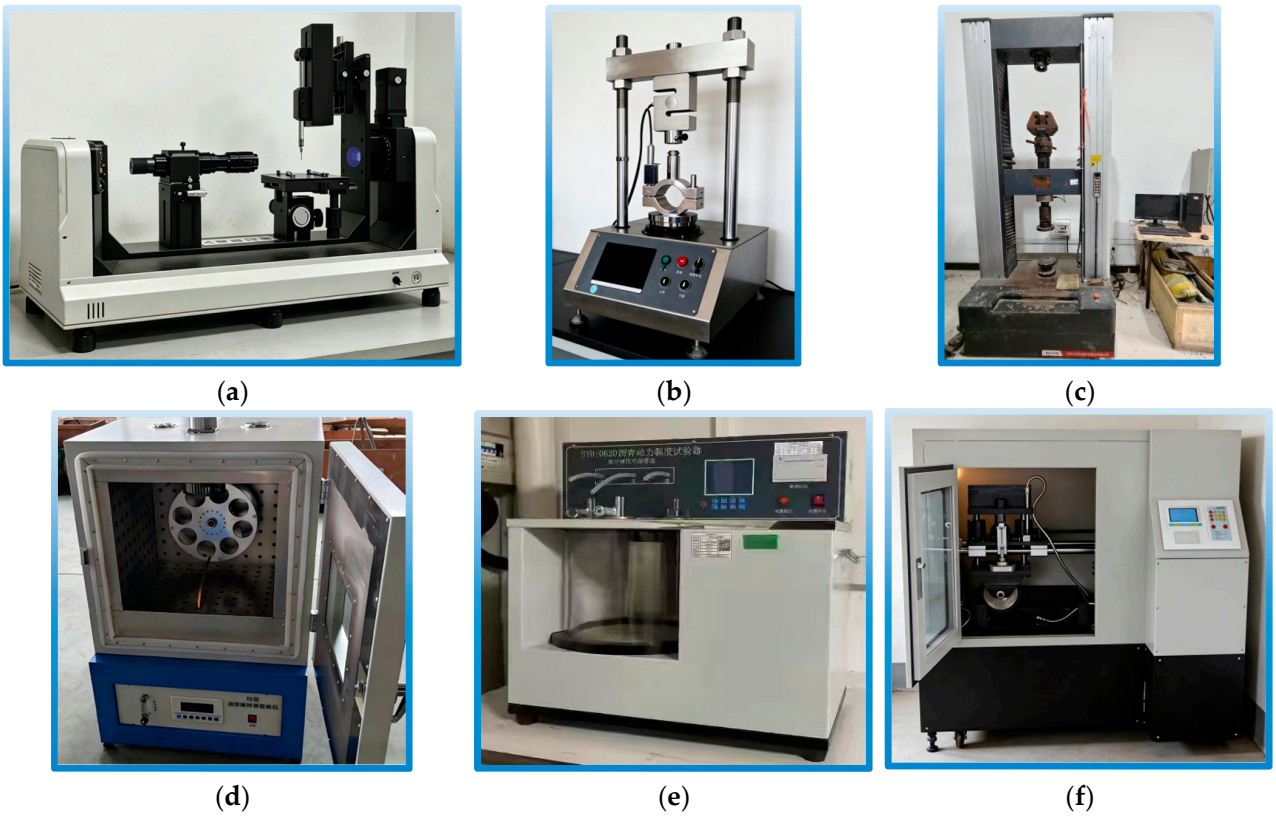


Figure 4. (**a**) Contact-angle meter; (**b**) Marshall stability tester; (**c**) electronic universal testing machine; (**d**) rolling thin-film oven; (**e**) asphalt dynamic viscosity tester; and (**f**) rutting tester.

The laboratory accelerated abrasion test was performed using an accelerated abrasion tester, as shown in Figure 5a. In this device, a reciprocating carriage drives a tire abrasion head to apply cyclic abrasion to the specimen surface, thereby simulating the degradation of skid resistance during long-term pavement service. The operating parameters were as follows: reciprocating stroke of 170 mm, cycling frequency of 13.5 cycles/min, and tire abrasion-head pressure of 0.25 MPa. After every 2 h of operation, the British Pendulum Number (BPN) of the specimen surface was measured and recorded using a pendulum friction coefficient tester, as shown in Figure 5b. The selection of these test parameters was based on the tire–pavement contact stress levels typical of urban roads and expressways. The tire–head contact pressure of 0.25 MPa falls within the standard inflation-pressure range of passenger car tires, approximately 0.20–0.30 MPa. The reciprocating frequency of 13.5 cycles/min corresponds to low-speed driving conditions and was intended to accelerate the abrasion process so that the long-term skid-resistance degradation of pavement could be reproduced within a laboratory time scale. Each 2 h testing interval corresponded to approximately 1620 reciprocating abrasion cycles, representing the long-term cumulative polishing action experienced by pavements under actual traffic.



(**a**) (**b**) (**c**)

Figure 5. (**a**) Accelerated abrasion tester; (**b**) pendulum friction coefficient tester; and (**c**) Cantabro particle-loss tester.

The immersion Cantabro particle-loss test was conducted using a TD733-1 asphalt mixture Cantabro particle-loss tester, as shown in Figure 5c. The torsional raveling test was also conducted using the same laboratory accelerated abrasion tester. This test introduces a rotational friction condition to simulate the combined kneading–torsional action exerted by tires on the pavement surface. The operating parameters were set as follows: reciprocating stroke of 170 mm, cycling frequency of 13.5 cycles/min, tire abrasion–head pressure of 0.07 MPa, and rotational friction speed of 390 r/min. The compound condition imposed in the torsional raveling test, in which reciprocating kneading is superimposed with rotational friction, was designed to approximate the coupled shear–torsional action exerted by tires on the pavement surface during vehicle turning, acceleration, deceleration, and braking. The relatively low contact pressure of 0.07 MPa reflects the stress level in the local slip zone of the tire tread during turning; the reciprocating stroke and frequency correspond to the tire slip recovery cycle under low-speed turning or braking; and the rotational friction speed simulates the circumferential shear component acting on the pavement surface when vehicles travel through curves or intersections.

3. Results and Discussion

3.1. Basic Properties of Composite High-Viscosity Modified Asphalt and Ceramic Aggregate Mixtures

3.1.1. Interfacial Adhesion and Wettability Between Asphalt and Ceramic Aggregates

Asphalt–aggregate interfacial adhesion is a critical factor governing the raveling resistance and long-term wear-retained skid performance of asphalt mixtures. Once interfacial bonding failure occurs, the asphalt film may strip from the aggregate surface, leading to particle loosening and detachment; this process can eventually develop into pavement raveling and pothole distress while accelerating the loss of skid-resistant texture. To clarify the effect of TPS composite high-viscosity modified asphalt on ceramic–asphalt interfacial bonding, this study compared T&S composite high-viscosity modified asphalt with SBS-modified asphalt using the water-immersion method, in accordance with the adhesion test method for coarse aggregates and asphalt specified in the *Technical Specifications for Construction of Highway Asphalt Pavements* [26]. In addition, to further quantify the wetting and spreading ability of asphalt on ceramic aggregate surfaces, contact-angle tests were conducted on the two asphalt systems using the sessile-drop method.

The results of the water-immersion adhesion test are shown in Figure 6. The adhesion grade between conventional SBS-modified asphalt and ceramic aggregates was only Grade 3 (The adhesion rating evaluation criteria are given in Table 8). The asphalt film on the aggregate surface exhibited pronounced stripping under hot-water erosion, indicating typical interfacial moisture damage. In contrast, the adhesion grade of the T&S composite high-viscosity modified asphalt reached Grade 5, with the stripped area of the asphalt film approaching zero. No identifiable stripping was observed under the same immersion conditions, demonstrating that the T&S-modified interface exhibited substantially better moisture stability than that of SBS-modified asphalt.



Figure 6. Asphalt adhesion evaluated by the water-immersion method.

Table 8. Adhesion grade evaluation criteria.

Asphalt Film Stripping Condition on Ceramic Aggregate Surface	Adhesion Grade
The stripped area of asphalt film is approximately zero	5
The stripped area of asphalt film is less than 10%	4
The stripped area of asphalt film is less than 30%	3
The stripped area of asphalt film is greater than 30%	2
The asphalt film is almost completely stripped, and asphalt floats on the water surface	1

As shown in Figure 7, the contact angles of all T&S groups were substantially smaller than those of the SBS control group at both test temperatures, indicating that TPS effectively reduced the contact angle of asphalt on ceramic surfaces and markedly improved the wetting and spreading ability of asphalt on ceramic aggregates. With increasing TPS dosage, the contact angle first decreased and then increased. The T&S-8 group exhibited the minimum values at both temperatures, 92.3° at 25 °C and 68.1° at 60 °C, which were approximately 16.2° and 17.6° lower than those of the SBS control group, respectively. The contact angles of the T&S-11 group, 94.8° at 25 °C and 69.7° at 60 °C, increased slightly relative to those of T&S-8, probably because excessive TPS increased system viscosity and reduced fluidity. This trend is consistent with the decline in ductility observed at the 11% TPS dosage. It is also noteworthy that the contact angles of all groups at 60 °C were markedly smaller than those at 25 °C, which is consistent with the enhanced flowability of asphalt at elevated temperature. Because this temperature approaches the high-temperature conditions during asphalt-mixture mixing and compaction, the contact

angle of only 68.1° for T&S-8 indicates excellent wetting and spreading on ceramic surfaces within the construction temperature range, facilitating the formation of a more uniform and complete interfacial asphalt film under practical construction conditions.

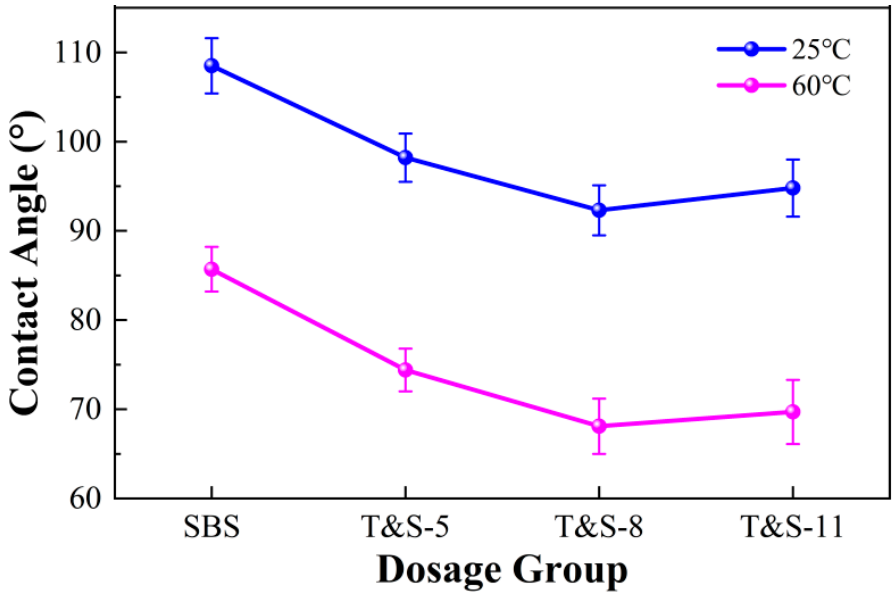


Figure 7. Contact angle between different asphalt binders and ceramic aggregates.

The enhancement of asphalt–ceramic aggregate interfacial adhesion by the TPS modifier can be explained from three perspectives. First, at the binder scale, TPS, SBS polymers, and asphalt components jointly form a stable three-dimensional interpenetrating network, which substantially increases the cohesive energy and 60 °C dynamic viscosity of the asphalt. The enhanced load-bearing capacity and resistance to water erosion of the asphalt film make it less susceptible to cohesive failure under hot-water immersion, thereby reducing the risk of film stripping at the source. Second, at the interfacial interaction scale, polar active groups on TPS molecular chains may develop strong interactions, such as hydrogen bonding or polar adsorption, with inorganic oxides containing silicon and aluminum on ceramic aggregate surfaces. The contact angle results support this inference from the perspective of wetting and spreading: the contact angle of T&S-8 at 60 °C was approximately 17.6° lower than that of SBS asphalt, indicating that TPS effectively enhanced the affinity of asphalt for ceramic surfaces. This interaction is stronger than the interface formed by SBS-modified asphalt, which relies primarily on van der Waals physical adsorption, and helps block the penetration of water molecules into the interface and to weaken water-induced displacement of the asphalt film, thereby improving the moisture stability of interfacial bonding to some extent [27]. Third, at the physical spreading scale, TPS provides the modified asphalt with excellent wetting and leveling abilities, enabling the asphalt to form a more homogeneous, complete, and continuous film on the rough and irregular ceramic aggregate surface. This reduces interfacial defects and potential pathways for water intrusion, further strengthening the long-term stability of the interface [28].

The above improvements in interfacial adhesion and wettability mainly explain the advantages of T&S high-viscosity asphalt from the binder perspective. However, the pore structures of the ceramic aggregates themselves also have a non-negligible influence on long-term interfacial stability. Drawing on studies of nanopore evolution and moisture-sensitive responses in clay-based materials, open pores and crushing-induced microcracks on ceramic aggregate surfaces may serve as rapid pathways for

moisture penetration into the interface under immersion conditions [29]. Once water molecules enter these nanoscale pores through capillary action, temperature variation or freeze–thaw cycling may generate expansion pressure and further promote the growth of interfacial microcracks. In this study, the water absorption of the ceramic aggregates was 0.86%, corresponding to an estimated open porosity of approximately 2.1%. Although this value is much lower than that of highly porous recycled aggregates, it still indicates a certain moisture-storage capacity. During the immersion Cantabro test (48 h, 60 °C), moisture may penetrate through open pores to the aggregate–asphalt interfacial region and weaken the bonding strengthened by T&S high-viscosity asphalt. This helps explain why the immersion particle-loss ratios of mixtures with high ceramic aggregate contents (≥60%) still increased markedly even when Grade 5 adhesion was achieved with T&S asphalt (Figure 6). It should also be noted that pore structures vary considerably among ceramic aggregates from different sources. High-temperature-sintered tile waste typically exhibits lower open porosity (<1%), whereas low-temperature-sintered daily-use or sanitary ceramics may contain higher open porosity (2–5%). Therefore, when the mix design recommended in this study is applied to other types of waste ceramics, mercury intrusion porosimetry or nitrogen adsorption is recommended to characterize pore features, and the asphalt content should be adjusted accordingly to compensate for asphalt absorbed by open pores or more stringent interfacial reinforcement measures should be adopted.

It should be emphasized that the ceramic aggregates used in this study were derived from waste generated during the production of daily-use ceramic products by Wuzhou Tengxian Xinzhongtao Co., Ltd., Wuzhou, China. Their chemical composition was dominated by SiO_2 (68.5 wt%) and Al_2O_3 (19.2 wt%), with an average surface roughness Ra of 5.2 ± 0.8 μm and a water absorption of 0.86%. These values represent only the typical characteristics of daily-use ceramic waste. According to the systematic review of multi-source solid-waste ceramic materials by Li et al. [19], waste ceramics from different sources, such as sanitary ceramics, ceramic tiles, and electrical porcelains, exhibit substantial variations in chemical composition: SiO_2 may range from 64 to 73 wt%, Al_2O_3 from 16 to 22 wt%, and fluxing oxides such as CaO, MgO, K_2O, and Na_2O may vary more markedly (e.g., CaO: 0.5–3.0 wt%; K_2O: 2.5–5.0 wt%). These compositional differences directly affect liquid-phase formation during sintering and the density of polar functional sites on ceramic surfaces, thereby modifying the wetting behavior and adhesion strength at the asphalt–aggregate interface. For example, higher CaO or MgO contents may promote the formation of alkaline sites on ceramic surfaces, which can alter their interactions with acidic components in asphalt. In addition, differences in crushing processes, including jaw crushing and impact crushing, and sintering temperature can also change the density of surface microcracks and the open porosity of ceramic aggregates. Therefore, the conclusion that TPS-modified asphalt improves the interfacial adhesion and wettability of ceramic aggregates is most applicable to bulk daily-use ceramic waste systems. When this material system is extended to other specific waste ceramic aggregates, such as polished tile waste or electrical porcelain waste, targeted adhesion-grade evaluation and contact-angle testing are still recommended to verify its applicability boundary.

In summary, incorporation of the TPS modifier improves the interfacial adhesion between asphalt and ceramic aggregates through enhanced binder cohesion, stronger interfacial interactions, and improved physical spreading. In particular, the 8% TPS dosage performed best in both adhesion grade, Grade 5, and contact angle, 68.1° at 60 °C, further supporting its rationality as the preferred dosage under the present experimental conditions. This provides a performance basis for improving the moisture damage resistance and

raveling resistance of ceramic aggregate high-viscosity asphalt mixtures. However, because pore structure and surface chemistry vary among different waste ceramic sources, the laboratory findings should be validated before being extended to other ceramic aggregate systems or field applications.

3.1.2. Conventional Properties of Composite High-Viscosity Modified Asphalt

As shown in Table 9, with increasing TPS dosage, the penetration of the composite modified asphalt at 25 °C gradually decreased from 54 × 0.1 mm for the SBS control group to 41 × 0.1 mm for the T&S-11 group, indicating a continuous increase in asphalt consistency and resistance to shear deformation at ambient temperature. The ring-and-ball softening point increased monotonically from 72 °C to 98 °C, reflecting a substantial improvement in high-temperature flow-deformation resistance. The ductility at 5 °C first increased and then decreased with increasing TPS dosage. The T&S-8 group reached a peak value of 40 cm, representing a 42.9% increase compared with the SBS control group. Although the ductility of the T&S-11 group decreased slightly to 37 cm, it remained 32.1% higher than that of the control group. This trend indicates that an appropriate TPS dosage can further toughen the SBS-modified asphalt network and improve the low-temperature flexibility of the binder. However, excessive TPS dosage may cause the crosslinking density of the system to approach saturation, restricting chain-segment mobility and resulting in a moderate decrease in ductility, although the value remains markedly higher than that of the SBS control asphalt.

Table 9. Basic properties of composite high-viscosity modified asphalt binder.

Dosage Group	Penetration/0.1 mm	Softening Point/°C	Ductility/cm
SBS	54	72	28
T&S-5	46	86	34
T&S-8	43	95	40
T&S-11	41	98	37

The 60 °C dynamic viscosity is a key indicator for evaluating the bonding ability and aggregate-coating capacity of high-viscosity asphalt, and is directly related to the wear-retained skid performance and raveling resistance of asphalt mixtures. The dynamic viscosity results at different TPS dosages are shown in Figure 8. The dynamic viscosity of SBS-modified asphalt was very low and far below the technical threshold for high-viscosity asphalt. As the TPS dosage increased, the 60 °C dynamic viscosity of the composite-modified asphalt exhibited an approximately exponential increase. The values for the T&S-5, T&S-8, and T&S-11 groups reached approximately 45,000 mPa·s, 102,000 mPa·s, and 180,000 mPa·s, respectively, all far exceeding the lower technical limit for high-viscosity asphalt. This behavior can be attributed to the full swelling and expansion of the TPS polymer network in the continuous asphalt phase, which markedly increases the cohesive strength and flow resistance of the system. Meanwhile, the interpenetrating network structure significantly enhances intermolecular interactions within the asphalt, providing essential binder-level support for the pavement performance of the mixture. Although viscosity growth endows asphalt with excellent high-temperature bonding performance, it also imposes more stringent requirements on mixture mixing, paving, and compaction. Excessive viscosity may reduce mixing uniformity, increase paving resistance, and make it difficult to ensure compaction. Therefore, a rational balance is required between performance enhancement and construction feasibility. The 8% TPS dosage was located in the optimal range in terms of both 60 °C dynamic viscosity and ductility, while its viscosity was not high enough to seriously impair construction

workability; thus, it is recommended as a dosage that balances pavement performance and field operability.

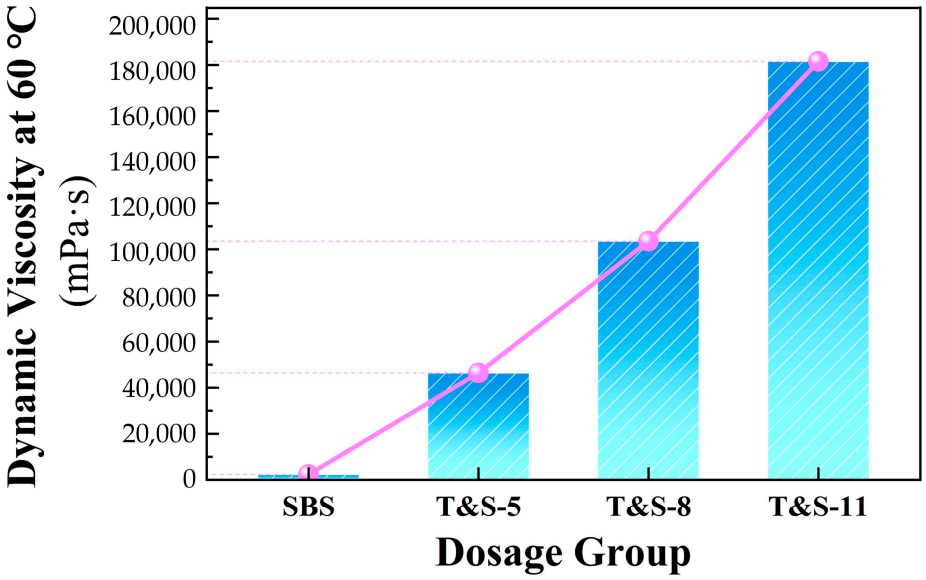


Figure 8. Test results of 60 °C dynamic viscosity.

The evolution of these conventional properties essentially reflects the molecular-scale structural synergy between TPS and SBS. From the perspective of polymer-blend compatibility, TPS and SBS both contain styrenic blocks and conjugated diene segments, and they are therefore expected to form a relatively homogeneous blend under high-temperature shearing, with limited tendency toward macroscopic phase separation. More importantly, polar active groups on TPS molecular chains, such as ester and hydroxyl groups, may interact with the polybutadiene segments of SBS and the polar fractions of asphalt, including oxygen- and nitrogen-containing groups in resins and asphaltenes, through hydrogen bonding or dipole–dipole interactions. Together with physical chain entanglement, these weak interactions may form a semi-interpenetrating-polymer-network-like (semi-IPN-like) structure. This network increases the cohesive energy and 60 °C dynamic viscosity of asphalt on the one hand, and helps maintain elastic recovery on the other, as indirectly supported by the improved ductility and residual ductility after aging. Nevertheless, storage-stability and phase-separation tests were not conducted in this study, and this aspect should be verified in future work.

Thermo-oxidative aging resistance is a key factor controlling the long-term performance stability of modified asphalt. The RTFOT results used to simulate short-term thermo-oxidative aging during mixing and paving are listed in Table 10 [30]. As the TPS dosage increased, the retained penetration ratio after aging increased from 72.2% for the SBS group to 92.1% for the T&S-11 group; the residual ductility at 5 °C increased from 18 cm to a maximum of 33 cm for the T&S-8 group; and the absolute mass change decreased from 0.49% to 0.23%. These three indicators were all superior to those of the SBS control asphalt. To further interpret the underlying mechanism, this study draws on the oxidation-resistance framework proposed by Zhu et al. for polymer-modified asphalt, in which oxygen quenching and VOC adsorption are considered important stabilization pathways [31]. The aging resistance of the TPS–SBS system may be explained by three synergistic mechanisms. First, the physical barrier effect: the interpenetrating network formed by TPS and SBS creates a dense physical barrier in the continuous asphalt phase, prolonging oxygen diffusion paths and suppressing the volatilization of light components. This is supported by the lower absolute mass loss of T&S-8 compared

with SBS after RTFOT aging (0.32% versus 0.49%). Second, possible radical stabilization: aromatic structures and unsaturated bonds in TPS molecular chains may stabilize free radicals generated during aging through π–π conjugation, thereby slowing chain oxidation reactions. This mechanism is similar in concept to the sacrificial antioxidant behavior reported for lignin-modified asphalt, but should be regarded here as a mechanistic inference rather than direct chemical proof. Third, light component retention: the very high 60 °C dynamic viscosity of T&S-8, approximately 102,000 mPa·s, provides strong physical restraint on light asphalt fractions, reducing VOC release and helping maintain the colloidal stability of asphalt.

Table 10. Properties of residues after RTFOT aging.

Dosage Group	Retained Penetration Ratio/%	Ductility/cm	Mass Change/%
SBS	72.2	18	−0.49
T&S-5	85.4	29	−0.36
T&S-8	89.5	33	−0.32
T&S-11	92.1	32	−0.23

These mechanisms are not isolated but mutually reinforcing. The physical barrier reduces oxygen diffusion, possible radical stabilization consumes active oxidative species that have entered the binder, and light component retention helps preserve the integrity of the asphalt colloidal structure. Together, these effects provide a plausible binder-level explanation for the improved thermo-oxidative aging resistance of TPS–SBS composite high-viscosity asphalt. This advantage supports the robustness of the binder during mixing and paving and may contribute to the performance retention of ceramic aggregate high-viscosity asphalt mixtures under coupled thermal, moisture, and mechanical actions. However, because only RTFOT aging was evaluated, longer-term aging tests such as PAV should be considered in future work.

Overall, the experimental results and mechanistic analysis indicate that the TPS modifier improved the conventional properties, high-viscosity characteristics, and short-term aging resistance of SBS-modified asphalt in a consistent direction. Under the present test conditions, T&S-8, corresponding to an 8% TPS dosage, achieved the best balance among high-temperature softening resistance, low-temperature flexibility, 60 °C dynamic viscosity, and residual ductility after aging. Its viscosity was also not so high as to seriously impair construction workability. Therefore, T&S-8 was selected as the preferred binder for the subsequent pavement performance evaluation of ceramic aggregate high-viscosity asphalt mixtures.

3.1.3. Overview of the Basic Pavement Performance of Ceramic Aggregate Mixtures

T&S modified asphalt was prepared using the previously identified optimum TPS dosage of 8%. Ceramic aggregates were then used to replace limestone aggregates at an equal volume, and asphalt mixtures with different ceramic aggregate contents were prepared to comparatively evaluate mixture performance under the synergistic effects of ceramic aggregates and high-viscosity modified asphalt.

The density of the ceramic aggregate was lower than the specification requirement, and its influence on mixture performance is two-sided. On the favorable side, the low density can reduce mixture self-weight and decrease dead-load stress in pavement structures; the equal-volume replacement scheme eliminates the interference of density differences with the gradation skeleton, and both the crushing value and abrasion value satisfy the specification requirements. On the unfavorable side, low density combined with relatively high water absorption, 0.86%, increases the optimum asphalt content and therefore material

cost. Moreover, the larger specific surface area per unit mass of aggregate increases the total asphalt–aggregate interfacial area, imposing higher requirements on water sensitivity and long-term raveling resistance. This is the key reason why T&S high-viscosity asphalt was adopted in this study to reinforce interfacial bonding. These trade-offs indicate that applying ceramic aggregates in asphalt pavements is not a simple replacement of natural aggregates by waste materials; rather, systematic optimization is required in skeleton design, asphalt dosage, interfacial reinforcement, and dosage control.

As shown in Figure 9, the dynamic stability of both the SBS control group and the T&S test group decreased continuously with increasing ceramic aggregate content. However, at each dosage level, the DS value of the T&S group was consistently much higher than that of the SBS group. At 0% ceramic aggregate content, the DS value of the SBS group was 7054 passes/mm, whereas that of the T&S group reached 11,667 passes/mm, corresponding to an increase of approximately 65%. When the ceramic aggregate content increased to 80%, the T&S group still maintained a DS value of 2541 passes/mm, approximately 53% higher than that of the corresponding SBS group, which was 1658 passes/mm. The excellent high-temperature performance of the T&S group originates from the rheological advantages of its binder. The extremely high 60 °C dynamic viscosity and softening point of the composite high-viscosity asphalt provide the asphalt mastic with stronger resistance to shear flow, effectively suppressing shear deformation and aggregate slippage in the mixture under high-temperature loading. The gradual decline in dynamic stability with increasing ceramic aggregate content is mainly attributed to the relatively smooth surface and weaker angularity of ceramic aggregates compared with natural hard aggregates, which weakens stone-on-stone interlocking at high ceramic aggregate contents. Nevertheless, the strong bonding characteristics of T&S high-viscosity asphalt largely compensate for the loss of aggregate skeleton interlocking, resulting in significantly better high-temperature performance than that of the SBS control group across the full range of ceramic aggregate contents.

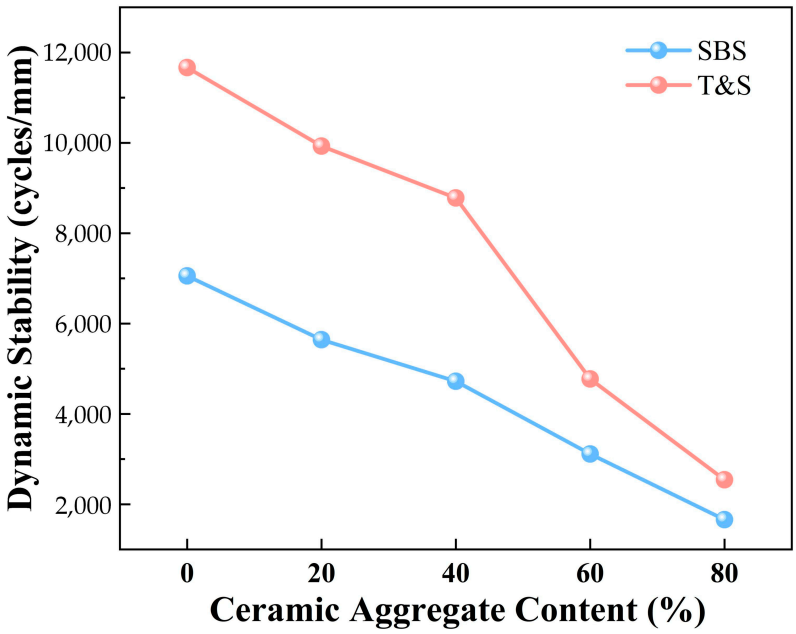


Figure 9. Effect of ceramic aggregate content on the dynamic stability of asphalt mixtures.

As shown in Figure 10, across the full range of ceramic aggregate contents, both moisture stability indicators of the T&S group were significantly higher than those of the SBS control group, and their degradation with increasing ceramic aggregate content was

much slower. At 0% ceramic aggregate content, the moisture stability of both mixtures satisfied the specification requirements. When the ceramic aggregate content increased to 60%, the residual Marshall stability and freeze–thaw splitting strength ratio of the SBS group decreased sharply to 67.0% and 62.1%, respectively, failing to meet the moisture stability requirements for high-grade highways. In contrast, the corresponding values of the T&S group remained at excellent levels of 88.8% and 87.7%, respectively. When the ceramic aggregate content further increased to 80%, the two indicators of the SBS group decreased to 52.7% and 47.2%, indicating an almost complete loss of moisture stability. By contrast, the T&S group still retained residual levels of 78.3% and 79.4%, respectively.

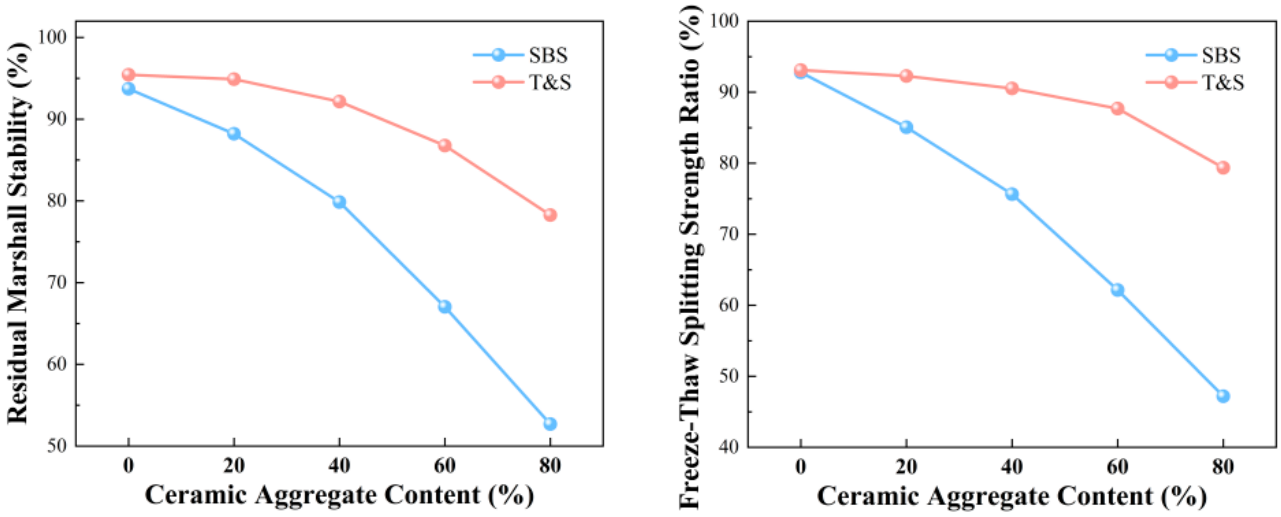


Figure 10. Effect of ceramic aggregate content on the moisture stability of asphalt mixtures.

Moisture damage is essentially caused by water intrusion into the asphalt–aggregate interface, which induces asphalt film stripping and bonding failure. The superior moisture stability of the T&S group can be attributed to the synergy of two mechanisms. First, the extremely high viscosity and cohesion of the composite high-viscosity asphalt enable it to form a thicker and denser asphalt film on the aggregate surface, providing much stronger resistance to water penetration and stripping than SBS-modified asphalt. Second, possible interfacial interactions, including polar adsorption and hydrogen-bonding interactions between the polar groups on TPS molecular chains and the aggregate surface improve the resistance of the interface to displacement by water molecules. The decrease in moisture stability at high ceramic aggregate contents is attributable to the increasing proportion of weak interfaces as the ceramic aggregate content rises. However, the strong bonding effect of T&S high-viscosity asphalt effectively mitigates this deterioration trend and broadens the safe dosage window for ceramic aggregates.

As shown in Figure 11, at each ceramic aggregate content, the indirect tensile strength of the T&S group was much higher than that of the SBS control group, and its degradation rate with increasing ceramic aggregate content was considerably lower. At 0% ceramic aggregate content, the strength of the SBS group was 1.69 MPa, whereas that of the T&S group reached 2.53 MPa, representing an increase of approximately 50%. At ceramic aggregate contents of 20% and 40%, the strengths of the T&S group remained at 2.50 MPa and 2.44 MPa, respectively, with no significant deterioration. When the ceramic aggregate content increased to 80%, the strength of the T&S group decreased to 0.85 MPa, but it remained approximately 37% higher than that of the corresponding SBS group, which was 0.62 MPa. The overall mechanical advantage of the T&S group originates from the substantial enhancement of bonding at the high-viscosity asphalt mastic–aggregate interface. The strengthened interface enables more

uniform stress transfer within the mixture under loading, delaying the initiation and propagation of microcracks and thereby improving the overall tensile resistance. The strength reduction at high ceramic aggregate contents indicates that the negative effect of weakened aggregate skeleton interlocking gradually exceeds the positive contribution of enhanced asphalt bonding. Nevertheless, the presence of high-viscosity asphalt significantly slows this degradation process.

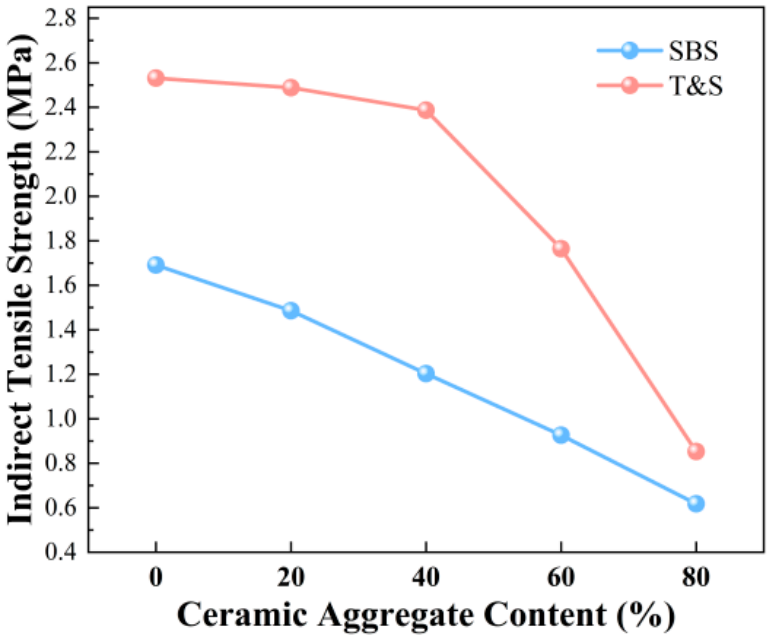


Figure 11. Effect of ceramic aggregate content on the indirect tensile strength of asphalt mixtures.

3.2. Wear-Retained Skid Performance of Ceramic Aggregate High-Viscosity Asphalt Mixtures

3.2.1. Wear-Retained Skid Performance

According to the *Field Test Methods of Subgrade and Pavement for Highway Engineering* (JTG E60-2008) [32], the measured pendulum values were temperature-corrected and uniformly converted to the standard value at 20 °C. The correction equation is expressed as follows:

$$BPN_{20} = BPN_t + \Delta BPN \quad (1)$$

where BPN_{20} is the standard pendulum value at 20 °C, BPNt is the measured pendulum value at temperature t, and ΔBPN is the temperature correction value, as listed in Table 11.

Table 11. Temperature correction values for BPN.

Temperature/°C	0	5	10	15	20	25	30	35	40
ΔBPN	−6	−4	−3	−1	0	+2	+3	+5	+7

In terms of initial skid resistance, the BPN at 0 h increased steadily with increasing ceramic aggregate content. The control group with 0% ceramic aggregate exhibited a BPN of 65.6, whereas the BPN values of the 20–80% groups ranged from 66.8 to 70.2; the 80% group showed an increase of approximately 7.0% compared with the control group. This improvement can be attributed to the high hardness of ceramic aggregates and the abundant microtexture on their fractured surfaces. Compared with limestone aggregates, ceramic particles provide greater interfacial frictional resistance, thereby directly enhancing the skid-resistant texture of the pavement surface.

During 16 h of continuous abrasion, the BPN values of all groups exhibited nonlinear degradation, characterized by rapid attenuation in the early stage followed by a slower decline in the later stage. The 0–8 h interval corresponded to the rapid abrasion stage of protruding aggregate surface textures, during which BPN decreased rapidly. During 8–16 h, the aggregate surface gradually became smoother, and the attenuation rate correspondingly decreased. Although all groups followed a similar overall trend, substantial differences were observed in attenuation magnitude and final retention rate. After 16 h of abrasion, the BPN of the control group decreased to 30.0, corresponding to a total attenuation of 54.3% and a performance retention rate of only 45.7%, indicating the weakest long-term skid resistance. The final BPN of the 20% group was 32.7, with an attenuation of 51.0%, suggesting that the reinforcing effect at low ceramic aggregate content remained limited. The final BPN of the 40% group increased markedly to 37.1, with the attenuation decreasing to 45.4% and the performance retention rate increasing to 54.6%, indicating a pronounced improvement in skid resistance. The final BPN values of the 60% and 80% groups reached 40.2 and 41.6, respectively, and the attenuation further decreased to 41.5% and 40.7%, indicating the best long-term skid-retention capacity. However, the improvement became noticeably less pronounced beyond the 40% ceramic aggregate content.

The relationship between ceramic aggregate content and BPN after 16 h of abrasion in Figure 12 shows a clear two-stage growth pattern, from which 40% ceramic aggregate content can be identified as a critical inflection point for improving long-term skid resistance. Within the 0–40% range, the curve exhibited a relatively steep slope, and the final BPN increased by an average of approximately 3.55 units for every 20% increase in ceramic aggregate content, indicating that the skid resistance reinforcement effect of ceramic aggregates was fully mobilized. In the 40–80% range, the slope decreased markedly, and the average increment dropped to 2.25 units, reflecting diminishing marginal benefits. This inflection point can be explained as follows: when the ceramic aggregate content is below 40%, highly wear-resistant ceramic aggregates progressively replace limestone, rapidly improving the overall abrasion resistance of the aggregate system. Once the content exceeds 40%, the mixture has essentially formed a ceramic-dominated skid-resistant skeleton, and the abrasion resistance of the aggregate system approaches the intrinsic upper limit of ceramic aggregates, leaving limited room for further improvement.

The improvement in wear-retained skid resistance provided by ceramic aggregates results from the combined effect of their intrinsic abrasion resistance and the aggregate-coating capacity of T&S high-viscosity asphalt. Ceramic aggregates delay surface texture polishing, whereas the high-viscosity binder helps suppress particle loosening and early detachment, thereby maintaining skid-resistant texture under the present laboratory abrasion conditions. From an engineering applicability perspective, the 20% group provided limited reinforcement, whereas the 60% and 80% groups showed better skid-retention capacity but also clear diminishing marginal benefits and higher material cost. The 40% group achieved a reasonable balance among skid-resistance improvement efficiency, service stability, and economy under the present test conditions. It should be noted, however, that the skid-resistance evaluation was based on a laboratory accelerated abrasion test. The abrasion conditions used in this study, namely a constant load of 0.25 MPa, a rubber abrasion head, dry contact, and a constant temperature of $20 \pm 2\ ^{\circ}C$, differ from actual pavement environments. In field service, tire type and inflation pressure, pavement temperature fluctuations (-30 to $60\ ^{\circ}C$), rainwater lubrication, deicing salts, and braking or turning actions may all affect the skid-resistance degradation rate. Therefore, the BPN degradation curves in Figure 12 reflect rela-

tive trends under the present laboratory conditions rather than absolute predictions of field performance. The ranking of mixtures with different ceramic aggregate contents (80% > 60% > 40% > 20% > 0%) is informative, but the extrapolation of specific degradation rates to the field should be treated cautiously.

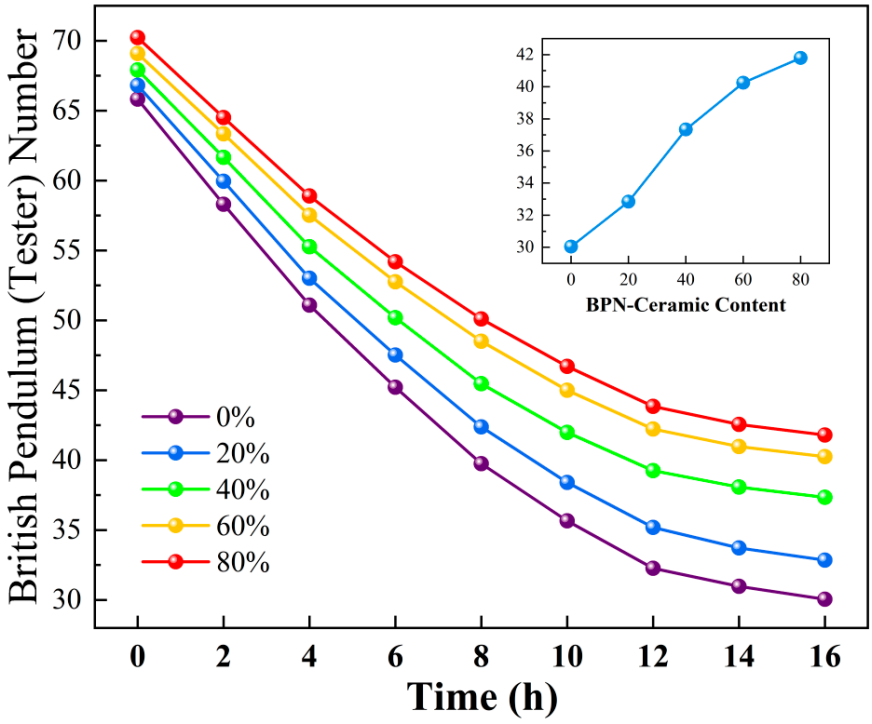


Figure 12. Variation in BPN of mixtures with different ceramic aggregate contents as a function of abrasion time.

3.2.2. Empirical Model for Skid-Resistance Degradation

The service-stage evolution of asphalt pavement skid resistance generally exhibits nonlinear characteristics, including rapid degradation in the early stage, slower degradation in the middle stage, and stabilization in the later stage. To quantitatively describe the degradation of BPN with abrasion time for ceramic aggregate high-viscosity asphalt mixtures, a three-parameter negative exponential model commonly used in road engineering was fitted to the time-series data obtained from the laboratory accelerated abrasion test [33]. The model is expressed as follows:

$$BPN(t) = A_t + B_t e^{-c_t t} \quad (2)$$

where t is the accelerated abrasion duration, h; BPN(t) is the pendulum value at the corresponding time; At is the long-term stable limit value, corresponding to the residual BPN after the mixture reaches a stable abrasion state; Bt is the total attenuation amplitude, defined as the difference between the initial BPN and At; and ct is the degradation rate constant, h^{-1}, with a larger value indicating faster degradation.

Parameter optimization was performed using the Levenberg–Marquardt nonlinear least-squares algorithm [34], with the constraints $A_t > 0$, $B_t > 0$, and $c_t > 0$. The fitting results are listed in Table 12. The coefficients of determination, R^2, of the five mixture groups were all no lower than 0.9978, indicating an excellent agreement between the model and the experimental data.

Table 12. Fitting parameters of the skid-resistance degradation model.

Ceramic Aggregate Content	Stable Value At	Attenuation Amplitude Bt	Degradation Rate Constant ct/h^{-1}	R^2
0%	27.84	38.10	0.132	0.9978
20%	30.11	36.97	0.124	0.9982
40%	34.85	33.22	0.115	0.9986
60%	37.65	31.59	0.108	0.9988
80%	39.42	30.96	0.102	0.9989

The evolution of the model parameters with ceramic aggregate content quantitatively reveals the mechanism by which ceramic aggregates improve skid-resistance durability from three perspectives. First, the stable limit value A_t increased monotonically with ceramic aggregate content, from 27.84 at 0% to 39.42 at 80%, directly quantifying the residual skid resistance after long-term service and indicating that ceramic aggregates can effectively raise the safety lower limit of pavement skid resistance. Second, the total attenuation amplitude B_t decreased monotonically with increasing ceramic aggregate content, from 38.10 to 30.96, indicating that higher ceramic aggregate contents reduce the total skid-resistance loss over the full service cycle and improve performance stability. Third, the degradation rate constant c_t decreased monotonically from 0.132 h^{-1} to 0.102 h^{-1}, reflecting the continuous inhibitory effect of ceramic aggregates on the abrasion-induced degradation rate.

Notably, the magnitude of parameter variation also supports the identification of 40% ceramic aggregate content as the threshold for a performance leap. In the 0–40% range, c_t decreased by 12.9%, and A_t increased by 25.2%; whereas in the 40–80% range, the corresponding decrease and increase narrowed to 11.3% and 13.1%, respectively. This diminishing marginal improvement is highly consistent with the experimental analysis in Section 3.2.1.

3.2.3. Frictional Impulse-Based Characterization Model for Skid-Resistance Degradation

Although the time-based empirical model established in the previous section provides high fitting accuracy for the laboratory data, its parameters depend on the specific abrasion condition, namely constant load, dry contact, constant temperature, and fixed abrasion media. Therefore, the model cannot be directly generalized to different loading and contact conditions. Drawing on the validation logic commonly used in combined experimental and numerical studies of structural reinforcement, this section attempts to construct a skid-resistance degradation characterization model using cumulative frictional impulse I as the basic variable and, more importantly, to define its applicability and predictive boundaries [35]. The model is intended to describe the present laboratory data and to compare the relative polishing resistance of different mixtures, rather than to provide direct field-life prediction [36].

According to JTG E60-2008, the standard BPN at 20 °C can be converted to the pavement sliding friction coefficient μ as follows:

$$\mu = \frac{BPN}{100} \tag{3}$$

In this test, a constant contact pressure of 0.25 MPa was applied, and the effective contact area between the abrasion wheel and the specimen remained fixed; therefore, the

normal load F_N was constant. The sliding friction force is determined by the friction coefficient and the normal load:

$$F_f = \mu \cdot F_N = \frac{BPN}{100} \cdot F_N \tag{4}$$

The friction impulse ***I*** is defined as the time integral of the sliding friction force:

$$I = \int_0^t F_f d\tau = \frac{F_N}{100} \int_0^t BPN(\tau) d\tau \tag{5}$$

Substituting the empirical skid-resistance degradation model established in Section 3.2.2 into the integral and solving it yields the analytical relationship between cumulative friction impulse and abrasion duration:

$$I = \frac{F_N}{100} \left[A_t t + \frac{B_t}{c_t} \left(1 - e^{-c_t t}\right) \right] \tag{6}$$

This establishes a quantitative relationship among abrasion time, friction impulse, and skid resistance. Based on this relationship, the cumulative friction impulse and corresponding BPN values of mixtures with different ceramic aggregate contents at different abrasion times were calculated. The results showed that the degradation of BPN with I also followed a three-parameter negative exponential form. Accordingly, a mechanical model with friction impulse as the independent variable was constructed as follows:

$$BPN = A + Be^{-I/C} \tag{7}$$

where I is the cumulative friction impulse, kN·h; A is the long-term stable limit value; B is the total attenuation amplitude; and C is the characteristic degradation constant, kN·h. A larger C value indicates slower skid-resistance degradation with cumulative friction impulse and stronger polishing resistance of the material.

The same algorithm as that used in Section 3.2.2 was adopted for fitting, with the constraints A > 0, B > 0, and C > 0. The fitting results are shown in Table 13 and Figure 13.

Table 13. Fitting parameters of the skid-resistance degradation model based on ***I***.

Ceramic Aggregate Content	Stable Limit Value A	Attenuation Amplitude B	Characteristic Degradation Constant C/kN·h	R^2
0%	27.84	38.10	0.340	0.9978
20%	30.11	36.97	0.362	0.9982
40%	34.85	33.22	0.390	0.9986
60%	37.65	31.59	0.415	0.9988
80%	39.42	30.96	0.440	0.9989

The R^2 values were all higher than 0.997, indicating high fitting accuracy for the present laboratory data set. The model parameters have clear descriptive meanings under the tested abrasion condition. The stable limit value A increased monotonically with ceramic aggregate content, indicating that ceramic aggregates increased the residual skid-resistance level after laboratory abrasion. The total attenuation amplitude B decreased monotonically, suggesting that skid-resistance loss under the present test condition was suppressed. The characteristic degradation constant C increased from 0.340 kN·h to 0.440 kN·h, providing a quantitative index for comparing the relative polishing resistance of the mixtures.

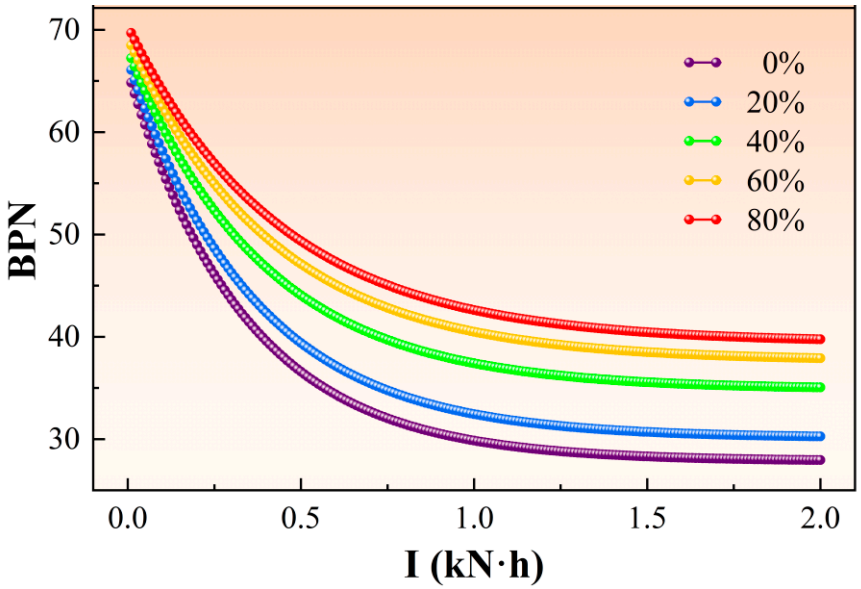


Figure 13. Fitted curves of the skid-resistance degradation model based on ***I***.

Furthermore, according to the characteristic constant C, the abrasion process of the mixture can be divided into three characteristic stages, which are fully consistent with the curve shapes in Figure 13. When I < 3C, the mixture is in the rapid abrasion stage, during which protruding surface textures are quickly worn down and BPN decreases sharply and approximately linearly; this is the core stage of pavement skid-resistance loss. When 3C < I< 6C, the mixture enters the stable abrasion stage, during which the surface gradually becomes smoother, the degradation rate decreases substantially, and the curve tends to flatten. When I > 6C, the ultimate stable stage is reached, BPN approaches A, and skid resistance no longer decreases significantly. From the parameter comparison, the C values of the groups with ceramic aggregate contents of 40% and above were significantly higher than those of the low-content groups. These mixtures could enter the stable abrasion stage earlier and exhibited higher stable limit values A, which is reflected in Figure 13 by fitted curves that consistently lie above those of the low-content groups, indicating superior residual skid resistance under laboratory constant-load abrasion conditions.

Considering both model parameters and engineering applicability, the 0% and 20% low-content groups degraded rapidly and had low stable limits, making them inadequate for long-life pavements. Although the 80% group exhibited the best polishing resistance, its marginal benefits diminished, material costs increased, and construction workability was also affected. Compared with the 20% group, the 40% group showed an increase of approximately 7.7% in C and 15.7% in A, demonstrating the most prominent efficiency in improving skid resistance. It achieved a rational balance among durability, economy, and construction performance, corroborating the conclusions drawn above. The 60% group is more suitable for pavement sections with special skid-resistance requirements and lower cost sensitivity, such as heavy-duty traffic sections and long, steep grades.

It should be noted that the high goodness of fit of the above model partly results from the inherent self-consistency of the data association, because it was converted from BPN. To preliminarily examine the applicability of the model under variable loading conditions, additional accelerated abrasion tests were conducted on the T&S mixture with 40% ceramic aggregate content, which exhibited favorable overall performance in this study, under two additional normal loads of 0.15 MPa and 0.35 MPa. Together with the reference load of 0.25 MPa, three loading conditions were considered. Continuous

abrasion was performed for 16 h under each loading condition, BPN was recorded every 2 h, and two parallel specimens were tested for each condition.

Two approaches were adopted for model validation. The first was parameter stability verification: if model parameter C has physical significance in reflecting the intrinsic polishing resistance of the material, it should remain relatively stable under different load levels. Increasing the load accelerates BPN degradation, but the intrinsic resistance of the material to polishing should not change fundamentally with load. The second approach was cross-prediction validation: the fitting parameters (A0, B0, C0) obtained under the 0.25 MPa reference load were used to predict the BPN degradation curves under the 0.15 MPa and 0.35 MPa loads, and the coefficient of determination R^2 between predicted and measured values was calculated to quantitatively evaluate cross-load prediction accuracy.

As shown in Table 14, the coefficient of variation of parameter C under the three load levels was 3.5%, indicating good parameter stability within this load range. Under the 0.15 MPa and 0.35 MPa loads, the cross-prediction R^2 values reached 0.985 and 0.978, respectively, showing good agreement between predicted and measured values. These results suggest that the frictional impulse-based skid-resistance degradation characterization model has a certain degree of cross-load applicability within the normal-load range of 0.15–0.35 MPa, and that parameter C can be used as a relative index of polishing resistance within this range. However, this verification was conducted using the same apparatus under adjacent load levels and should not be interpreted as independent field validation.

Table 14. Model validation results under different normal loads for the T&S mixture with 40% ceramic aggregate content.

Normal Load/MPa	Fitting Parameter C/kN·h	R^2 of Fitting	Cross-Prediction R^2
0.15	0.405	0.9975	0.985
0.25 (reference)	0.390	0.9986	-
0.35	0.378	0.9970	0.978

It should be emphasized that the above model has clear boundaries. First, the model can describe the BPN decay with cumulative frictional impulse under the specified laboratory conditions: 0.25 MPa, dry contact, 20 ± 2 °C, and a rubber abrasion head. Parameter C can be used to quantify relative polishing resistance, with a larger C corresponding to a slower decay rate; in this study, C increased from 0.340 to 0.440 kN·h as ceramic aggregate content increased from 0% to 80%. Second, the model cannot directly predict the field skid-resistance degradation rate or pavement service life, because it does not account for temperature fluctuations, moisture, tire type, braking, turning, acceleration, freeze–thaw cycling, or wet abrasion. It also cannot replace full-scale accelerated loading tests or long-term field monitoring. Third, the load dependence of parameter C was only preliminarily examined under 0.15, 0.25, and 0.35 MPa. Although the coefficient of variation of C was 3.5% and the cross-prediction R^2 values were not lower than 0.978, this validation was limited to different load conditions within the same device and was not calibrated against field data. Therefore, uncertainty will increase substantially when the model is applied beyond this load range or to wet, freeze–thaw, or temperature-varying conditions.

The main value of the frictional impulse-based skid-resistance degradation characterization model is therefore threefold: (i) it provides a unified quantitative framework for describing skid-resistance decay of mixtures with different ceramic aggregate contents under laboratory constant-load abrasion; (ii) it enables relative ranking of material polishing resistance through parameter C; and (iii) it provides a quantitative basis for mix-design

optimization under the present test conditions. Its broader cross-condition applicability should be further verified through full-scale accelerated loading tests and long-term field data.

3.3. Raveling Resistance of Ceramic Aggregate High-Viscosity Asphalt Mixtures

3.3.1. Immersion Cantabro Particle-Loss Test

Raveling resistance is fundamental to the long-term service stability of asphalt mixtures. It directly determines the ability of pavement surfaces to resist aggregate loss, surface pitting, and pothole distress, and is also essential for maintaining the integrity of skid-resistant surface texture and delaying skid-resistance degradation [37]. To systematically evaluate the raveling resistance of ceramic aggregate high-viscosity asphalt mixtures under coupled moisture-loading conditions, the immersion Cantabro particle-loss test was conducted in accordance with the Standard *Test Methods of Bitumen and Bituminous Mixtures for Highway Engineering* (JTG E20-2011) [25]. Standard Marshall specimens were immersed in a constant-temperature water bath at 60 °C for 48 h, and then subjected to the particle-loss test using a Los Angeles abrasion machine. The particle-loss ratio was used as the evaluation index to investigate the effects of ceramic aggregate content and binder type on mixture raveling resistance. The test results are shown in Figure 14.

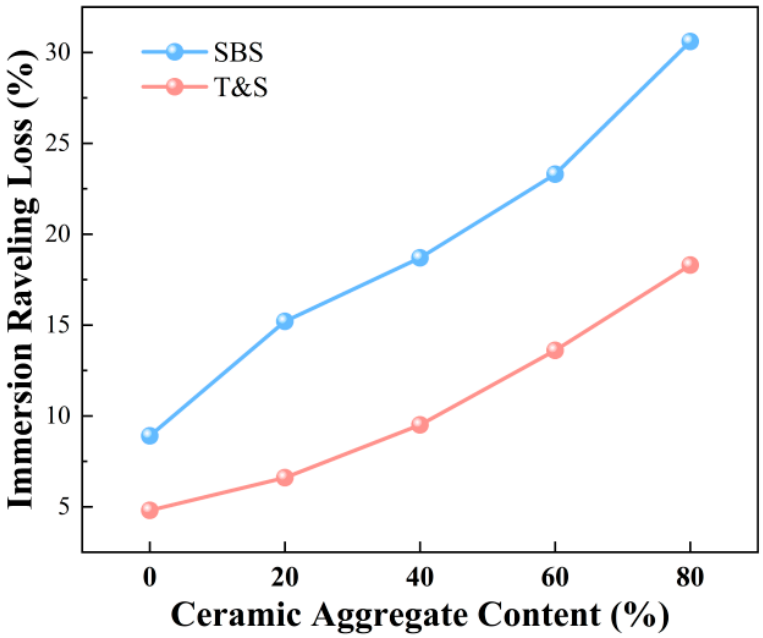


Figure 14. Immersion Cantabro particle-loss ratios of mixtures with different ceramic aggregate contents.

Under the same binder system, the immersion Cantabro particle-loss ratio increased continuously with increasing ceramic aggregate content. This is mainly because, compared with natural limestone aggregates, ceramic aggregates exhibit weaker angularity on fractured surfaces, more equiaxed particle shapes, and less abundant surface microtexture, resulting in an inherent deficiency in mechanical interlocking among aggregates. As the equal-volume replacement ratio of ceramic aggregates increases, the proportion of aggregates with strong interlocking capacity in the skeleton structure decreases, making particle loosening and detachment more likely under impact loading and consequently increasing particle loss.

More importantly, at all ceramic aggregate contents, the particle-loss ratio of the T&S composite high-viscosity modified asphalt mixture was significantly lower than that of the SBS control group. At 0% ceramic aggregate content, the particle-loss ratio of the T&S group was approximately 46% lower than that of the SBS group. Within the 20–80% content range, the reductions were approximately 57%, 49%, 42%, and 40%, respectively. Even under the unfavorable condition of 80% ceramic aggregate content, the T&S group still exhibited much better raveling resistance than the SBS reference group. This comparison is highly consistent with the adhesion test results in Section 3.1.1, and the mechanism can be explained from two aspects. First, the adhesion grade between T&S asphalt and ceramic aggregates reached Grade 5, far exceeding the Grade 3 achieved by SBS asphalt; moreover, the contact-angle test confirmed its superior wetting and spreading ability on ceramic surfaces, with the contact angle at 60 °C approximately 17.6° lower than that of SBS asphalt. Under the coupled effects of long-term hot-water immersion and impact loading, the interface was less prone to water-film displacement and adhesive debonding, thereby suppressing particle loss at its origin. Second, the three-dimensional interpenetrating network jointly formed by TPS and SBS substantially enhanced the cohesion and impact toughness of the asphalt mastic, making cohesive failure less likely under loading and effectively maintaining the bonding integrity of the aggregate skeleton.

The above analysis mainly explains the improvement in raveling resistance from the binder side; however, moisture damage is also closely associated with the microstructural characteristics of the ceramic aggregate itself. During high-temperature sintering and mechanical crushing, a certain number of microcracks and open pores may form on the ceramic aggregate surface. These defects provide potential pathways for water to penetrate into and remain within the interfacial region. Drawing on the concept of the interfacial transition zone, ITZ, in composite materials, the ceramic–asphalt interface can be regarded as a structurally heterogeneous weak region: the aggregate side is a porous surface containing micro-defects, whereas the asphalt side is polymer-modified mastic. The abrupt transition in chemical composition and mechanical modulus between the two sides makes this region a preferential site for damage initiation under coupled hydro-mechanical action. Therefore, the moisture stability of the mixture depends not only on the chemical affinity and physical coating of asphalt for aggregates, but also on the pore and microcrack characteristics of the aggregate itself.

From the perspective of the dosage threshold, within the range of 0–40%, the particle-loss ratio of the T&S group increased only slightly from approximately 4.8% to 9.5%, with an increase of less than 5 percentage points, and remained below 10% throughout, fully satisfying the technical requirements for raveling resistance in high-grade highways. When the ceramic aggregate content increased from 40% to 80%, the particle-loss ratio further increased from approximately 9.5% to 18.3%, indicating a clearly accelerated deterioration rate. This trend indicates that a ceramic aggregate content of 40% is also a critical threshold for mixture raveling resistance. This finding agrees with the previously identified inflection point for wear-retained skid performance and further confirms that, at this content, the mixture achieves an optimal balance among wear-retained skid resistance, raveling resistance, and economy.

In summary, the immersion Cantabro particle-loss test confirms that TPS composite high-viscosity modified asphalt can partly compensate for the inherent interfacial bonding deficiency of ceramic aggregates and substantially improve the moisture-damage resistance and raveling resistance of ceramic aggregate asphalt mixtures, providing supporting evidence for their technical application in long-life skid-resistant pavements.

3.3.2. Torsional Raveling Test

To further evaluate the raveling resistance of the mixtures under repeated shear–kneading conditions, a torsional raveling test was conducted using the laboratory accelerated abrasion tester [38]. This loading condition was designed to simulate the combined kneading–torsional action exerted by tires on the pavement surface, which more closely reflects the complex stress states caused by frequent vehicle turning, acceleration, and deceleration during actual service. The time-dependent particle-loss mass at each stage was used as the evaluation index [37], and the test results are shown in Figure 15.

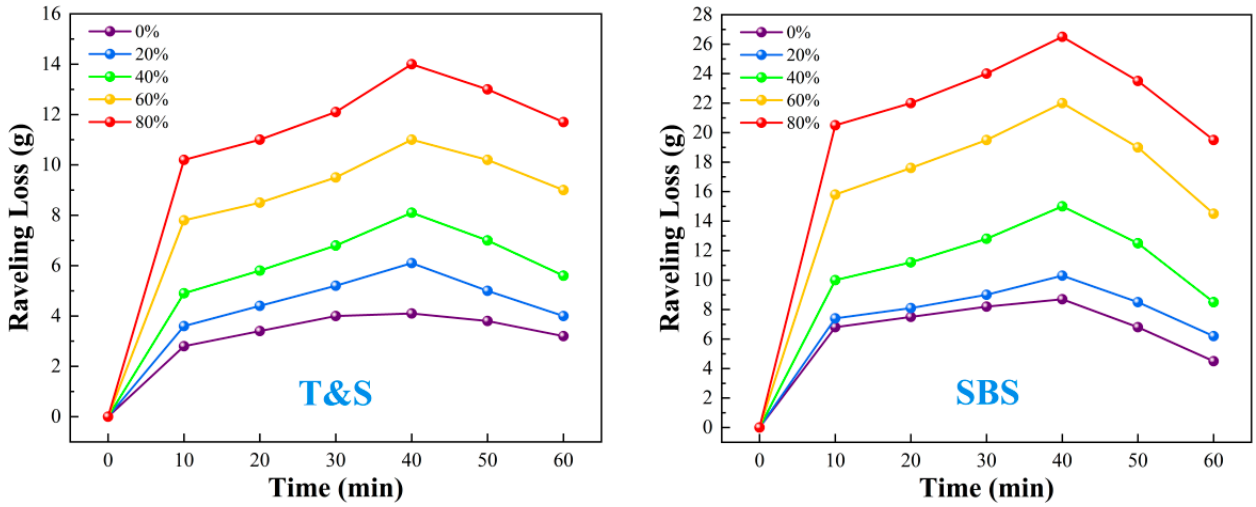


Figure 15. Time–history curves of torsional particle-loss mass for mixtures with different ceramic aggregate contents.

In terms of the time–history evolution, the particle-loss mass of all mixture groups showed a consistent pattern: it first increased continuously, reached a peak at approximately 40 min, and then gradually decreased. The period of 0–40 min corresponds to the rapid aggregate-detachment stage. Under repeated kneading–shear action, fatigue damage continuously accumulates at the asphalt–aggregate interface, interfacial bonding gradually deteriorates, and particles with weak interlocking and poor bonding within the skeleton loosen and detach first. As a result, particle loss increases continuously with loading time and reaches a peak at approximately 40 min. The period of 40–60 min corresponds to the performance stabilization stage. At this stage, easily detachable aggregates have largely been removed, while the remaining particles are firmly bonded to the asphalt and the aggregate skeleton remains stable. Therefore, the additional particle loss induced by continued kneading is substantially reduced, the measured particle-loss mass gradually decreases from its peak, and the raveling resistance tends to stabilize.

Under the same binder system, both the particle-loss mass at each stage and the total loss over the full test period increased monotonically with increasing ceramic aggregate content. The total loss of the SBS group increased from 42.5 g at 0% ceramic aggregate content to 136.0 g at 80%, corresponding to an increase of approximately 220%. For the T&S group, the total loss increased from 21.3 g to 72.0 g, corresponding to an increase of approximately 238%. This pattern is consistent with the results of the immersion Cantabro particle-loss test. The underlying mechanism is that the relatively weaker angularity and surface roughness of ceramic aggregates reduce the interlocking capacity of the aggregate skeleton. At high ceramic aggregate contents, the mechanical anchorage is further weakened, making particle sliding and detachment more likely under kneading loading [39].

In terms of the binder modification effect, the particle-loss mass of the T&S group was consistently much lower than that of the SBS group at the same ceramic aggre-

gate content. At 0% ceramic aggregate content, the total loss of the T&S group was approximately 49.9% lower than that of the SBS group. Within the 20–80% content range, the reductions were approximately 42.8%, 45.4%, 48.3%, and 47.1%, respectively, with improvements approaching 50% across the entire range. Even under the unfavorable condition of high ceramic aggregate content, 80%, the T&S group still maintained good resistance to kneading-induced raveling. This difference originates from two core advantages of T&S asphalt. First, its Grade 5 adhesion with ceramic aggregates endows the interface with stronger resistance to fatigue-induced debonding, thereby suppressing the causes of particle detachment at their origin. Second, the three-dimensional interpenetrating network jointly formed by TPS and SBS substantially enhances the cohesion and shear-fatigue resistance of the asphalt mastic, enabling the skeleton structure to maintain bonding integrity for a longer period under repeated kneading. In addition, the elastic-modulus mismatch between ceramic aggregates and asphalt mastic at the interface is significant. Under repeated kneading–shear action, this modulus mismatch can induce interfacial stress concentration and accelerate fatigue-damage accumulation. Surface microcracks generated during aggregate crushing may further amplify this effect and become initiation sites for interfacial debonding. Therefore, although T&S high-viscosity asphalt effectively delays raveling by enhancing interfacial adhesion and mastic cohesion, surface physical defects of the aggregate itself remain potential factors affecting long-term interfacial durability.

The above torsional raveling results reveal the overall raveling resistance of ceramic aggregate high-viscosity asphalt mixtures under repeated shear–kneading action. However, it should be noted that the test simulates only a short-term accelerated loading condition (60 min) and does not cover the more complex long-term fatigue process experienced by pavements in service. Drawing on the concept of interfacial transition zone (ITZ) degradation in cement-based composites under repeated environmental loading, the long-term durability limitations of the present mixture can be interpreted by analogy [40]. In cement-based composites, the aggregate–matrix interface is often the preferential site for thermal-fatigue damage initiation; differences in thermal expansion induce cyclic stress concentration, leading to microcrack initiation, pore coarsening, interfacial debonding, and ultimately macroscopic performance degradation. Similarly, in ceramic aggregate high-viscosity asphalt mixtures, the large difference in modulus and thermal expansion between ceramic aggregates (approximately 4–6 $\times$ 10^{-6}/°C) and asphalt mastic (approximately 15–20 $\times$ 10^{-5}/°C) may induce progressive fatigue damage accumulation in the interfacial region under daily temperature cycles and traffic loading. The torsional raveling test in this study captured a response characterized by an initial increase followed by stabilization in particle loss, but the 60 min accelerated test can represent only a limited number of turning or braking events. It cannot fully reflect the gradual accumulation of interfacial microdamage or the risk of sudden failure over years of service. Therefore, the favorable raveling resistance observed under the present test conditions should be interpreted as a potential short-term mechanical resistance rather than fully verified long-term service reliability.

From the perspective of the critical threshold, within the 0–40% content range, the total loss of the T&S group increased only from 21.3 g to 38.2 g, an increase of approximately 16.9 g (Figure 16). Notably, the total loss of the 40% group, 38.2 g, was still lower than the baseline value of the SBS group without ceramic aggregates, 42.5 g, indicating that the torsional raveling resistance of the T&S mixture at this content was even better than that of the ceramic-free SBS reference mixture. However, when the ceramic aggregate content further increased from 40% to 80%, the total loss rose sharply from 38.2 g to 72.0 g, an increase of approximately 33.8 g, indicating a clearly accelerated deterioration rate. This

pattern agrees well with the inflection-point conclusions obtained from the immersion particle-loss test and the wear-retained skid resistance analysis, further confirming that 40% is the key balance point for ceramic aggregate content.

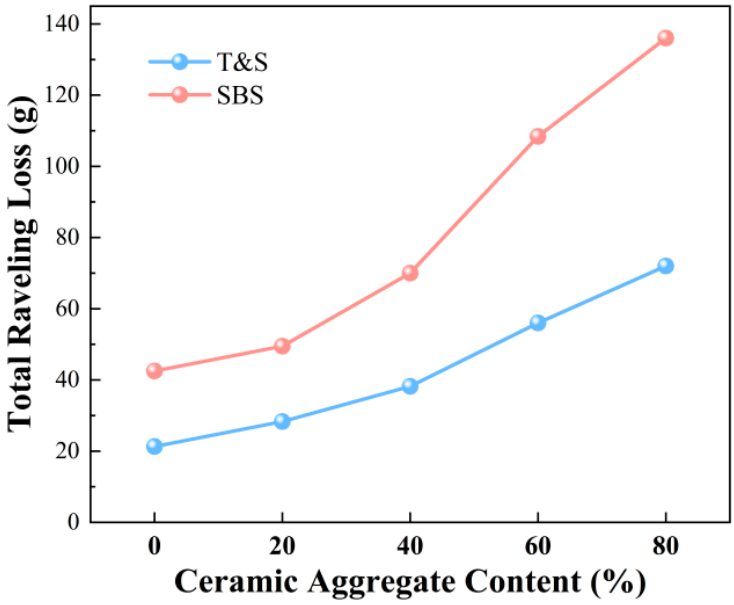


Figure 16. Total torsional particle loss of different modified asphalt mixtures at various ceramic aggregate contents.

The results suggest that TPS–SBS composite high-viscosity modified asphalt can partly compensate for the interlocking deficiency of ceramic aggregates and maintain favorable raveling resistance under repeated shear action in the laboratory. These findings provide useful performance evidence for the potential use of ceramic aggregate high-viscosity asphalt mixtures in pavement friction courses, but field validation is still required before broader engineering application.

3.4. Multi-Criteria Comprehensive Decision Analysis of Ceramic Aggregate Content

The preceding sections evaluated the pavement performance of T&S high-viscosity asphalt mixtures with different ceramic aggregate contents from the perspectives of skid resistance, raveling resistance, high-temperature stability, moisture stability, and mechanical properties. The results indicate that different performance indicators evolved differently as ceramic aggregate content increased: skid resistance increased monotonically, high-temperature performance decreased monotonically, and moisture stability and raveling resistance deteriorated only slowly at low contents but deteriorated more rapidly at high contents. Because the optimum content corresponding to a single indicator differs among performance dimensions, it is necessary to establish a multi-criteria decision-making framework to systematically balance different performance requirements and determine a ceramic aggregate content with favorable overall performance.

3.4.1. Construction of the Evaluation Matrix

Seven indicators were selected to construct the multi-criteria performance evaluation matrix: residual BPN after 16 h of abrasion, representing skid-resistance durability; immersion raveling loss, representing moisture-induced raveling resistance; total torsional raveling loss, representing mechanical raveling resistance; dynamic stability, representing high-temperature performance; freeze–thaw splitting strength ratio, representing moisture stability; indirect tensile strength, representing mechanical performance; and optimum asphalt content, representing economy. The solid-waste utilization

rate, expressed as ceramic aggregate content, was also included as a reference dimension. The weighting assignment was based on the functional positioning of a long-life skid-resistant surface layer: skid resistance, raveling resistance, and moisture stability were assigned the highest priority; high-temperature performance and mechanical performance were assigned intermediate priority; and economy and solid-waste utilization were treated as reference priorities.

3.4.2. Comprehensive Performance Analysis and Mechanical Response Mechanism

As shown in Table 15, as the ceramic aggregate content increased from 0% to 80%, the mixture exhibited a clear trade-off among different performance indicators. The 0% control group had the best mechanical and durability indicators in the series, but its skid resistance was the lowest, with a residual BPN after 16 h of only 30.0, and it could not exploit the wear-resistant advantage of ceramic aggregates. The 20% group showed the highest durability retention, with an immersion raveling loss of only 6.9% and a freeze–thaw splitting strength ratio of 93.3%, but its skid-resistance gain was limited, with the residual BPN only 2.7 units higher than that of the control group. The 60% and 80% groups reached residual BPN values of 40.2 and 41.6, respectively, but durability deterioration accelerated: for the 60% group, the immersion raveling loss increased to 13.5%, the total torsional raveling loss increased to 56.0 g, and dynamic stability decreased to 4773 passes/mm; for the 80% group, the performance imbalance was more pronounced, and several indicators approached or fell below engineering safety margins. By contrast, the 40% group achieved a favorable balance among key dimensions: its residual BPN, 37.1, was approximately 23.7% higher than that of the control group; the immersion raveling loss, 9.5%, remained below the commonly used engineering control limit of 10%; the total torsional raveling loss, 38.2 g, was lower than that of the SBS control group, 42.5 g; the decreases in freeze–thaw splitting strength ratio, 90.5%, and indirect tensile strength, 2.44 MPa, remained acceptable; and the optimum asphalt content, 4.8%, was clearly lower than that of the 60% group, 5.4%.

Table 15. Multi-criteria performance evaluation matrix for different ceramic aggregate contents.

Evaluation Aspect	Evaluation Indicator	0%	20%	40%	60%	80%	Weight
Skid durability	Residual BPN (16 h)	30.0	32.7	37.1	40.2	41.6	★★★
Raveling resistance (moisture)	Immersion raveling loss/%	4.8	6.9	9.5	13.5	18.2	★★★
Raveling resistance (mechanical)	Total raveling loss/g	21.3	28.3	38.2	56.0	72.0	★★☆
High-temperature performance	Dynamic stability/(passes/mm)	11,667	9926	8779	4773	2541	★★☆
Moisture stability	Freeze–thaw splitting strength ratio/%	93.1	93.3	90.5	87.7	79.4	★★★
Mechanical property	Indirect tensile strength/MPa	2.53	2.50	2.44	1.56	0.85	★★☆
Cost efficiency	Optimum asphalt content/%	4.3	4.5	4.8	5.4	6.1	★★☆
Solid-waste utilization	Ceramic content/%	0	20	40	60	80	★☆☆

Note: The number of stars indicates the relative importance of each indicator in the comprehensive decision-making process. ★★★ denotes high priority, ★★☆ denotes medium priority, and ★☆☆ denotes reference priority.

The preference for 40% ceramic aggregate content can also be supported from a mechanical response perspective rather than by solely comparing performance indices [41]. First, in terms of load-transfer path and skeleton stress distribution, when the ceramic aggregate content is below 40%, the high-hardness ceramic particles act mainly as dispersed reinforcing phases embedded in the limestone skeleton. Under abrasion loading, ceramic particles preferentially bear contact stress, and their high hardness delays plastic deformation and polishing of surface asperities, which explains the increase in initial BPN with

ceramic content. At this stage, the limestone skeleton still provides the main interlocking force, and stress transfer occurs mainly through the aggregate–mastic–aggregate path, with relatively dispersed interfacial damage. When the ceramic aggregate content exceeds 40%, ceramic particles begin to form a more continuous contact skeleton, and the load-transfer path tends to shift toward direct ceramic–ceramic contact. Because the angularity of the ceramic aggregates is weaker than that of limestone, the mechanical interlocking at ceramic–ceramic contact points decreases, and stress transfer depends more strongly on asphalt mastic. This increases interfacial stress concentration and helps explain the accelerated deterioration of raveling resistance at high ceramic aggregate contents.

Second, from the viewpoint of interfacial damage accumulation and self-stabilization, the modulus difference between ceramic aggregates (approximately 50–80 GPa) and asphalt mastic (approximately 0.1–1 GPa) can cause strain incompatibility under repeated loading. When the ceramic content is no higher than 40%, the limestone skeleton provides better deformation compatibility and part of the interfacial stress can be dissipated through the viscous flow of the mastic. When the content reaches 60% or higher, strain incompatibility is intensified and the rate of interfacial microcrack initiation and propagation increases, explaining the sharp increase in total torsional raveling loss from 38.2 g at 40% to 56.0 g at 60%. The time–history curves of torsional particle loss, which first increased and then stabilized, also indicate a damage self-stabilization process: weak interfacial regions fail successively in the early loading stage, and, after easily detachable particles are removed, the remaining skeleton forms a more stable stress redistribution network. Third, the 8% TPS dosage can be interpreted as a balance among bonding strength, deformation capacity, and construction flowability. At this dosage, the 60 °C dynamic viscosity (approximately 102,000 mPa·s), 5 °C ductility (40 cm), and residual ductility after RTFOT aging act synergistically: viscosity is sufficiently high to restrain aggregate slip, ductility is sufficient to dissipate interfacial stress and avoid brittle fracture, and the binder still retains deformation compatibility after aging. Therefore, the combination of 8% TPS and 40% ceramic aggregate is recommended as a preferred balance point under the present test conditions, rather than as a unique optimum for all performance dimensions. When engineering applications emphasize skid resistance, a 60% ceramic aggregate content may be considered; when durability is the primary objective, a 20% content may be more conservative.

4. Conclusions and Outlook

4.1. Conclusions

This study used waste ceramic aggregates as the aggregate phase and TPS–SBS composite high-viscosity modified asphalt (T&S) as the binder to investigate the wear-retained skid resistance and raveling resistance of ceramic aggregate high-viscosity asphalt mixtures. The main conclusions are summarized as follows.

(1) The three-dimensional interpenetrating network jointly formed by TPS and SBS increased the asphalt–ceramic aggregate adhesion grade from Grade 3 for SBS-modified asphalt to Grade 5. An 8% TPS dosage reduced the asphalt–ceramic contact angle at 60 °C from 85.7° to 68.1°, substantially enhancing wetting and spreading ability and facilitating the formation of a more uniform and complete interfacial asphalt film. This improvement in interfacial properties provides a critical basis for the moisture-damage resistance and raveling resistance of the mixture.

(2) A TPS dosage of 8% achieved the optimal balance among high-temperature performance, low-temperature flexibility, 60 °C dynamic viscosity, aging resistance, and construction workability. It was therefore identified as the optimum modifier dosage under the present experimental conditions.

(3) The skid resistance of the mixture increased markedly with ceramic aggregate content, and 40% was identified as a practical performance turning point under the present test conditions. The improvement efficiency was greatest within the 0–40% range, whereas marginal benefits decreased from 40% to 80%. The empirical skid-resistance degradation model and the frictional impulse-based characterization model both provided high fitting accuracy for the laboratory data. The latter can be used as a quantitative tool for comparing the polishing resistance of different material systems under laboratory constant-load abrasion conditions.

(4) T&S high-viscosity asphalt partly compensated for the interfacial adhesion and aggregate-interlocking deficiencies of ceramic aggregates, thereby improving the raveling resistance of the mixture under the present laboratory conditions. At all ceramic aggregate contents, the immersion Cantabro loss and total torsional raveling loss of the T&S mixtures were more than 40% lower than those of the corresponding SBS mixtures. The 40% ceramic aggregate content was also identified as the practical threshold beyond which raveling resistance deteriorated more rapidly.

(5) Based on a multi-criteria comprehensive evaluation, a TPS dosage of 8% and a ceramic aggregate content of 40% are recommended as the preferred mix design under the present experimental conditions. This combination provides a reasonable balance among skid-resistance improvement, raveling-resistance retention, and durability margin, rather than representing a unique optimum across all performance dimensions. When specific engineering applications prioritize a particular performance requirement, the dosage can be flexibly adjusted using the multi-criteria evaluation matrix proposed in this study.

4.2. Limitations and Future Work

This study has several limitations, which provide directions for future research.

(1) The skid-resistance evaluation in this study was mainly based on laboratory-accelerated abrasion tests. Although the friction impulse model enables the extension of actual service conditions, long-term performance validation through full-scale accelerated loading tests or field trial sections is still lacking [42]. In future work, trial pavement sections should be constructed to monitor the long-term skid-resistance degradation and raveling behavior of this mixture under the coupled effects of natural traffic loading and climatic conditions.

(2) For the torsional raveling simulation test, although the operating parameters, including pressure, rotational speed, and stroke, were designed with reference to actual tire action, a quantitative correlation with standardized specification-based tests has not yet been established [43]. Future studies could combine discrete element modeling with tire–pavement contact mechanics analysis to further calibrate the mechanical equivalence of this method [44,45].

(3) Multi-factor coupled long-term durability has not yet been verified. This study considered only selected laboratory loading and immersion conditions and did not cover coupled thermal–mechanical fatigue, freeze–thaw damage, chemical attack from deicing salts or acid rain, long-term ultraviolet aging, or construction variability. The recommended mixture, 8% TPS and 40% ceramic aggregate, performed well under the present experimental conditions, but its long-term durability in real multi-field environments should be further validated through full-scale accelerated loading, outdoor trial sections, and multi-factor coupled durability tests.

Author Contributions: B.T.: Conceptualization, resources, writing—review and editing. Q.Z.: Methodology, investigation, writing—original draft. T.Z.: Investigation, validation, formal analysis. W.Z.: Methodology, visualization, supervision. L.Z.: Investigation, data curation. All authors have read and agreed to the published version of the manuscript.

Funding: This research was supported by the Guangxi Key Laboratory of Green Building Materials and Construction Industrialization, Guilin, China, through the Guangxi Science and Technology Program (Grant No. AD25069101).

Data Availability Statement: The original contributions presented in this study are included in the article. Further inquiries can be directed to the corresponding author.

Conflicts of Interest: The authors declare that they have no known competing financial interests or personal relationships that could have influenced the work reported in this article.

References

1. Alnawmasi, N.; Alamri, M.; Jashami, H. Assessing Injury-Severity Outcomes in Wet-Pavement Conditions: Exploring the Impact of Pavement Skid Resistance through Temporal Analysis with Random Parameters and Heterogeneity in Means and Variances. *Transp. Res. Rec.* **2025**, *2679*, 50–77. [CrossRef]
2. Zong, Y.; Li, S.; Zhang, J.; Zhai, J.; Li, C.; Ji, K.; Feng, B.; Zhao, H.; Guan, B.; Xiong, R. Effect of Aggregate Type and Polishing Level on the Long-Term Skid Resistance of Thin Friction Course. *Constr. Build. Mater.* **2021**, *282*, 122730. [CrossRef]
3. Alafeef, K.; Sharaf, T.; Abbas, A.R. Characterization of Aggregate Susceptibility to Polishing Using the Micro-Deval Test. *Transp. Res. Rec.* **2025**, *2679*, 1146–1159. [CrossRef]
4. Peng, Y.; Zhao, T.; Zeng, Q.; Deng, L.; Kong, L.; Ma, T.; Zhao, Y. Interpretation of Stripping at the Bitumen-Aggregate Interface Based on Fluorescence Tracing Method. *J. Mater. Res. Technol.-JMRT* **2023**, *25*, 5767–5780. [CrossRef]
5. Deng, K.; Wang, D.; Tang, C.; Situ, J.; Chen, L. A Cumulative Damage Model for Predicting and Assessing Raveling in Asphalt Pavement Using an Energy Dissipation Approach. *Front. Struct. Civ. Eng.* **2024**, *18*, 949–962. [CrossRef]
6. Yan, C.; Li, Q.; Wang, J.; Yang, H.; Wu, Y. Evaluation for Long-Term Skid Resistance of Ultra-Thin Asphalt Overlay Based on Texture Characteristics. *Constr. Build. Mater.* **2024**, *438*, 137151. [CrossRef]
7. Qian, G.; Wang, Z.; Yu, H.; Shi, C.; Zhang, C.; Ge, J.; Dai, W. Research on Surface Texture and Skid Resistance of Asphalt Pavement Considering Abrasion Effect. *Case Stud. Constr. Mater.* **2024**, *20*, e02949. [CrossRef]
8. He, Y.; Wang, C.; Yang, X.; Fan, Z.; Lu, G.; Liu, P.; Wang, D. Skid Resistance Performance Analysis and Driving Safety Evaluation in the Full Life Cycle of Asphalt Pavement. *J. Transp. Eng. Part B-Pavements* **2024**, *150*. [CrossRef]
9. de Oliveira Sousa, N.; Diran de Sousa, A.C.; de Souza, L.L.; Pretti, A.F.; Magnol, R.V.; Strey, N.F.; Scandian, C. High-Stress Abrasion of Engineering Ceramics and Cermets. *Wear* **2025**, *570*, 205975. [CrossRef]
10. Sun, Y.; Zhang, X.; Chen, J.; Liao, J.; Shi, C.; Huang, C. Mixing Design and Performance of Porous Asphalt Mixtures Containing Solid Waste. *Case Stud. Constr. Mater.* **2024**, *21*, e03644. [CrossRef]
11. Andrzejuk, W.; Woszuk, A.; Barnat-Hunek, D. Adhesion of Asphalt to Natural Aggregates and Sanitary Ceramic Waste. *Materials* **2025**, *18*, 1201. [CrossRef] [PubMed]
12. Al-Kheetan, M.J. Waste Not, Want Not: Sustainable Use of Anti-Stripping-Treated Waste Ceramic in Superpave Asphalt Mixtures. *Sustainability* **2023**, *15*, 7579. [CrossRef]
13. Song, X.; Jiang, H.; Kosiba, Y.; Yoshino, H.; Shibata, H.; Nagatani, A.; Ueda, Y. Mechanical Properties of Styrene-Based Thermoplastic Elastomer Composites Filled with Hydroxylapatite. *Kobunshi Ronbunshu* **2009**, *66*, 356–363. [CrossRef]
14. Wang, D.; Feng, D.; Chen, Z.; Liu, Z.; Zhang, W.; Lei, J.; Yao, D.; Yi, J.; Pei, Z. Research on TPS-SBS Composite-Modified Asphalt with High Viscosity and High Elasticity in Cold Regions. *Coatings* **2025**, *15*, 108. [CrossRef]
15. Li, K.; Yan, X.; Wang, Y.; Ai, T.; Niu, Y.; Chen, Y. Design and Modification Mechanism of a Novel High-Viscosity Thermoplastic Polyurethane Modified Asphalt. *Constr. Build. Mater.* **2024**, *433*, 136585. [CrossRef]
16. Wang, T.; Chen, Z.; Hong, J.; Liao, Z.; Wang, D.; Yuan, D.; Zhang, Y.; Falchetto, A.C. Preparation and Properties of High-Viscosity Modified Asphalt with a Novel Thermoplastic Rubber. *Sustainability* **2023**, *15*, 12190. [CrossRef]
17. Vanegas, N.C.C.S.; García, A.G.; Guzmán, M.F.S.; Ruíz, D.D.P. Challenges and Opportunities for the Use of Asphalt Mix Prepared with Ceramic Solid Waste in Emerging Countries. *Eng. Trans.* **2024**, *72*, 309–326. [CrossRef]
18. Nie, Q.; Wu, B.; Wang, Z.; Dai, X.; Chen, L. Incorporation of Disposed Face Mask to Cement Mortar Material: An Insight into the Dynamic Mechanical Properties. *Buildings* **2024**, *14*, 1063. [CrossRef]

19. Li, T.; He, G.; Jiang, Z.; Duan, Y.; Liu, M. Research Advances and New Insights into Multi-Source Solid Waste-Derived Ceramic Foams. *Sustain. Mater. Technol.* **2025**, *45*, e01535. [CrossRef]
20. Toghroli, A.; Mehrabi, P.; Shariati, M.; Trung, N.T.; Jahandari, S.; Rasekh, H. Evaluating the Use of Recycled Concrete Aggregate and Pozzolanic Additives in Fiber-Reinforced Pervious Concrete with Industrial and Recycled Fibers. *Constr. Build. Mater.* **2020**, *252*, 118997. [CrossRef]
21. Li, X.; Zhu, X.; Yuan, F. Cationic Imidazole Compounds: Syntheses, Characterization, and Effects on the Asphalt Adhesion and Water Damage of Granite-Asphalt Mixtures. *J. Adhes. Sci. Technol.* **2025**, *40*, 1609–1626. [CrossRef]
22. Li, P.; Kong, L.; Mao, N.; Gu, C. Impact of Calcined Bauxite Aggregates on the Polishing Resistance and Skid Resistance Performance of SMA-7 Asphalt Mixtures. *PLoS ONE* **2025**, *20*, e0329579. [CrossRef] [PubMed]
23. Yang, S.Y.; Chen, G.L. Research on anti-raveling performance of asphalt concrete for aggregate loss pavement on expressway. *J. China Foreign Highw.* **2023**, *43*, 227–230. [CrossRef]
24. Nam, J.; Hwang, U.; Yang, X.; Kim, S.; Nam, J.-D. Optimization of Rubber Domain Morphology in Thermoplastic Elastomer Blends for Improved Resilience. *ACS Appl. Polym. Mater.* **2025**, *7*, 8538–8546. [CrossRef]
25. *JTG E20-2011*; Standard Test Methods of Bitumen and Bituminous Mixtures for Highway Engineering. China Communications Press: Beijing, China, 2011.
26. *JTG F40-2004*; Technical Specification for Construction of Highway Asphalt Pavements. China Communications Press: Beijing, China, 2004.
27. Fan, J.; Zhu, Y.; Ma, T.; Xu, G.; Ding, X. Interface Interaction between High Viscosity Asphalt and Aggregate: A Multi-Scale Study Based on Experiments and Molecular Dynamics Simulation. *Fuel* **2024**, *357*, 130045. [CrossRef]
28. Andrzejuk, W.; Szewczak, A.; Fic, S.; Łagód, G. Wettability of Asphalt Concrete with Natural and Recycled Aggregates from Sanitary Ceramics. *Materials* **2020**, *13*, 3799. [CrossRef] [PubMed]
29. Zheng, Y.; Baudet, B.A. Evolution of Nano-Pores in Illite-Dominant Clay during Consolidation. *Acta Geotech.* **2024**, *19*, 71–83. [CrossRef]
30. Wu, W.; Chen, B.; Chen, J.; Li, Z. Study on the Equivalence of Extended-RTFOT and RTFOT-PAV in Asphalt Long-Term Aging Simulation. *Constr. Build. Mater.* **2025**, *476*, 141239. [CrossRef]
31. Zhu, H.; Hu, M.; Zhang, Y.; Abudurahman, A.; Zhu, Y.; Cui, J. Microwave-Functionalized Sustainable Lignin to Enhance Asphalt Oxidation Resistance: An Oxygen Quenching and VOCs Adsorption Perspective. *Fuel* **2026**, *410*, 137855. [CrossRef]
32. *JTG E60-2008*; Field Test Methods of Subgrade and Pavement for Highway Engineering. China Communications Press: Beijing, China, 2008.
33. Liu, Y.-M.; Wang, L.; Yang, Z. Attenuation law and prediction model of skid-resistance performance of asphalt pavement. *J. Chang. Univ. (Nat. Sci. Ed.)* **2023**, *43*, 1–10. [CrossRef]
34. Fischer, A.; Izmailov, A.F.; Solodov, M.V. The Levenberg–Marquardt Method: An Overview of Modern Convergence Theories and More. *Comput. Optim. Appl.* **2024**, *89*, 33–67. [CrossRef]
35. Luo, Z.; Sinaei, H.; Ibrahim, Z.; Shariati, M.; Jumaat, Z.; Wakil, K.; Pham, B.T.; Mohamad, E.T.; Khorami, M. Computational and experimental analysis of beam to column joints reinforced with CFRP plates. *Steel Compos. Struct. Int. J.* **2019**, *30*, 271–280. [CrossRef]
36. D'Apuzzo, M.; Evangelisti, A.; Nicolosi, V. A Correlation Between Braking Tire Contact Friction Energy and Pavement Skid Deterioration. In Proceedings of the Transportation Research Board 98th Annual Meeting, Washington, DC, USA, 13–17 January 2019.
37. Wang, Y.; Li, M.; Li, H.; Wu, J.; Ye, M.; Liang, C. Research Progress on Aggregate Loss in Asphalt Pavement. *AIP Adv.* **2025**, *15*, 100701. [CrossRef]
38. Sun, C.; Li, P.; Niu, B.; Xu, Y.; Zhang, W. Structure Stability and Shear Failure Behaviors of Asphalt Mixtures from the Perspective of Aggregate Particle Migration. *Constr. Build. Mater.* **2023**, *408*, 133653. [CrossRef]
39. Yao, B.; Xu, H.; Wang, Y.; Guo, P.; Chen, X.; Xu, H.; Wang, C. Optimization of Aggregates Skeleton Using Laser-Scanning Technology and Discrete Element Method. *Constr. Build. Mater.* **2023**, *408*, 133731. [CrossRef]
40. Zeng, H.; Jin, M.; Li, W.; Du, F.; Wang, X.; Ma, Y.; Yang, H.; Xiang, Y.; Zhao, H.; Liu, J. Thermal-Fatigue Challenges in the Interfacial Transition Zone (ITZ) of Concrete: How Fly Ash Modulates Degradation? *Cem. Concr. Compos.* **2026**, *168*, 106500. [CrossRef]
41. Zhang, W.; Zhang, S.; Wei, J.; Huang, Y. Flexural Behavior of SFRC-NC Composite Beams: An Experimental and Numerical Analytical Study. *Structures* **2024**, *60*, 105823. [CrossRef]
42. Chen, Y.; Li, Z.; Wang, Y.; Liang, G.; Yang, X. A Review of Long-Term Skid Resistance of Asphalt Pavement. *Appl. Sci.* **2025**, *15*, 1895. [CrossRef]
43. Chen, B.; Yu, X.; Cai, Y.; Dong, F.; Huang, J. Research on the Migration Law of Aggregate Particles in the Compaction Process of Asphalt Mixture Based on Discrete Element Method. *Constr. Build. Mater.* **2024**, *445*, 137895. [CrossRef]

44. Fan, J.J. Study on the Skid Resistance Degradation of Asphalt Pavement Based on 3D Texture and Tire–Pavement Contact Interface. Master's Thesis, Xinjiang Agricultural University, Urumqi, China, 2025.
45. Cardenas, J.J.; Al-Qadi, I.L. Impact of Road Roughness on Tire-Pavement Contact Stresses during Vehicle Maneuvering. *J. Eng. Mech.* **2025**, *151*. [CrossRef]

Disclaimer/Publisher's Note: The statements, opinions and data contained in all publications are solely those of the individual author(s) and contributor(s) and not of MDPI and/or the editor(s). MDPI and/or the editor(s) disclaim responsibility for any injury to people or property resulting from any ideas, methods, instructions or products referred to in the content.